

# Probing the Gauge Content of Heavy Resonances with Soft Radiation

Ilmo Sung

*C.N. Yang Institute for Theoretical Physics, Stony Brook University  
Stony Brook, New York 11794-3840, USA*

## Abstract

The use of energy flow is investigated as a diagnostic tool for determining the color SU(3) representation of new resonances. It is found that the pattern of soft gluon radiation into a rapidity gap depends on color flow in the hard scattering, and reflects the gauge content of new physics. The massive soft anomalous dimension matrix for rapidity gap events is introduced for describing soft gluon emission analytically in heavy quark pair production. A gap fraction is used for quantifying the amount of soft radiation into the gap region. In general, the results illustrate that radiation is greater for a singlet resonance than for an octet. Especially, it is found that the quantitative difference is quite distinguishable for spin-1 resonances, depending on the gauge content in the new sector.

## 1 Introduction

QCD has been successfully tested in many hadronic processes at high energy. Current efforts in perturbative QCD have moved toward precision, to help gain accurate predictions for Standard Model processes in collider experiments as backgrounds to new physics. Precise prediction is a key to find new physics, because QCD events should be distinguished from signals in order to claim the discovery of new phenomena at colliders. In this paper, we show how to use factorized cross sections as a tool for analyzing the gauge content of new heavy particles.

Factorization is a statement of the quantum mechanical incoherence of short and long distance physics, and plays an important role in the use of perturbative QCD. Perturbative

calculations of factorized partonic cross sections depend on the separation of regions of momentum space. The three basic regions describe off-shell “hard” partons at short distances, energetic, on-shell “collinear” partons near the light cone, and long-wavelength, “soft” partons (see Ref. [1] for reviews and references therein). Once we obtain a factorized form of the cross section for a certain process, resummation can be achieved from the independence of physical quantities from factorization scales, which leads to evolution equations [2]. The evolution equations can be solved to resum large logarithmic corrections in terms of perturbative anomalous dimensions. Especially, the soft anomalous dimension matrix introduced in Refs. [3, 4], which is the main interest in this paper, allows us to describe soft gluon radiation systematically in hadronic collisions.

In the mid 1990’s, dijet rapidity gap events with anomalously low radiation in a wide interjet rapidity region for electron-proton collision were observed at HERA [5–7] and for proton-antiproton scattering at the Tevatron [8]. Such events were predicted from the exchange of two or more gluons in a color singlet configuration, which avoids color recombination between jets [9]. A quantitative explanation of these events in terms of factorizable cross sections was studied in Ref. [10], which discussed the dependence of the dijet cross section on energy flow,  $Q_c$ , into the central region, in terms of a soft function that is a matrix in the space of the possible color exchange at the hard scattering. A “gap” here refers to low energy flow  $Q_c$ . Since then, there have been various studies of gap events from this point of view. The soft anomalous dimension matrix, denoted by  $\Gamma_S$  below, for rapidity gap events, was calculated in Ref. [10], and used to resum the leading logarithmic contributions in Refs. [11, 12]. The soft anomalous dimension matrix for three jet rapidity gap processes was calculated in Refs. [13–15].

Cross sections computed from the soft anomalous dimension matrix organize “global” logarithms, following the terminology introduced in Ref. [16], and as such do not organize all logarithms of the gap energy. Non-global logarithmic contributions, mis-cancellations from secondary emission, discovered by Dasgupta and Salam [16], were resummed in the large  $N_c$  approximation [17]. More recently, Forshaw, Kyrieleis and Seymour have discovered new logarithmic contributions which they name “super-leading logarithms”, which do not seem possible to exponentiate by current techniques [18–20]. The contributions of these non-global logarithms, however, are generally not dominant [21, 22].

In this paper, we study the pattern of soft gluon radiation into a rapidity gap for the production of heavy particles in hadron-hadron scattering at leading order in the soft matrix,

$\Gamma_S$ , which resums global logarithms. The pattern depends on color flow in the hard scattering, and reflects the gauge content of new particles that participate in the process, for example, as  $s$ -channel resonances.

The results of this paper illustrate the use of energy flow, treated by perturbative QCD and factorization, as a diagnostic tool for determining the color SU(3) representation of new resonances, and the use of resummation for more precise cross sections. Previous work on soft gluon radiation for the study of new physics includes Ref. [23] for Higgs boson production in association with two hard jets, and Refs. [24, 25] for gluino and squark pair production, which describe resummed cross sections to provide more accurate predictions for signals.

There are many proposals for extensions of the Standard Model. These could provide solutions to the hierarchy problem, dark matter explanation, the origin of mass, etc. The most common feature of the models is that they include new heavy particles transforming under definite gauge groups. In many scenarios, we expect that they are created with  $\mathcal{O}(\text{TeV})$  mass via  $s$ -channel processes in hadron-hadron scattering. Possible processes with various spins and gauge groups of new heavy particles are studied and summarized in Ref. [26], which considers new sectors that decay into a top quark pair. There have been studies for identifying signals, including hadronic or leptonic decays from gauge Kaluza-Klein (KK) resonance states and from QCD background [27–34]. These studies show that the ability to distinguish signals especially from hadronic decays, which have much larger branching ratio than leptonic decays, depends on both how strongly the new sector is coupled to the Standard Model and to what extent signals and backgrounds are separated [35–42]. Also, various methods for spin measurements of the intermediate new particles have been suggested and discussed (see Ref. [43] for reviews and references therein).

Our study begins from this point. Once we succeed in distinguishing a resonance from backgrounds, a remaining task is to determine the SU(3) color gauge content of the resonance particle, denoted as  $V'$ . For simplicity we consider below two possibilities; color-singlet ( $Z'$ ) and color-octet ( $G$ ). Since we consider QCD radiation with total energy much less than resonance energy, our considerations do not depend on the details of the model. In this paper, we assume that the decay width is large enough that a hard function is an effective vertex. We will, however, discuss the consequences of a narrow resonance at the end of Secs. 3 and 6.

In many models there are gauge interactions whose coupling with a top quark pair is

enhanced in particular. These include models with a KK excited graviton, weak and strong gauge bosons in extra dimensions [44, 45], as well as heavy spin-0 particles in MSSM and two-higgs-doublet model (2HDM) [46, 47] and spin-1 coloron and axigluon [48]. Such new particles  $V'$  of mass  $M$  and spin ( $sp$ ) could show up as resonances in  $pp(\bar{p}) \rightarrow V'(M, sp) \rightarrow Q\bar{Q}$  at the Tevatron and the LHC. We may expect larger branching ratios for heavy quark pair production than for other channels such as massless dijets or dileptons, due to the small couplings of  $V'$  to light particles. This motivates the calculation of an analytic form describing soft gluon emission in heavy quark pair production. At the level of global logarithms, this is determined by the soft anomalous dimension matrices for rapidity gap processes involving massive particles. The “massive” soft anomalous dimension matrix for heavy pair production was studied in Refs. [49–57] for threshold resummation. In this paper, we extend this work to introduce the massive soft anomalous dimension matrix for rapidity gap cross sections, which will be used as a tool for our analysis.

Reference [10] studied rapidity gaps for a process in which  $t$ -channel exchange was dominant. The result indicates that, in the limit of a very large interjet region, the color singlet component dominates, with more radiation into the gap when the exchange is a color-octet. In this study, however, we might expect a different pattern of soft gluon radiation due to new heavy particle resonances in the  $s$ -channel rather than  $t$ -channel. The quantity of interest is the gap fraction, the ratio of the number of events for heavy quark pair production with a gap energy up to some value  $Q_0$  to the total number of events for the process. We will find a quantitative difference that is quite distinguishable and can be used for the study of the gauge content in the new sector. This difference, especially caused by the SU(3) color content, is related to “drag” effects in  $e^+e^-$  three-jet ( $q\bar{q}g$ ) events, compared to  $q\bar{q}\gamma$  events [58–60]. The color dipole configurations explain a surplus of radiation in the  $qg$  and  $\bar{q}g$  interjet regions for three-jet events, while radiation is enhanced in the  $q\bar{q}$  region for  $q\bar{q}\gamma$  events.

In this study, we do not give a detailed study of non-global [16] or super-leading logarithms [18], arising when gluons radiated outside the gap emit back into the gap. The latter are sometimes called secondary emissions. We can in principle introduce correlations between energy flow and event shapes that suppress such secondary emissions naturally. This technique was introduced in Ref. [61] for rapidity gap  $e^+e^-$  dijet events. Such correlations control secondary radiation, by suppressing states with radiation outside the gap at intermediate energy scales, leading to perturbatively computable measures insensitive to non-global

logarithms. In our study, the rapidity gap we choose does not allow radiation of high transverse momentum outside the gap by definition, which suppresses the non-global logarithms from final-state radiation. On the other hand, another issue arises for hadronic collisions, where there is secondary emission nearly parallel to the initial partons. Several classes of observables studied in Refs. [62–64] could be used to suppress exponentially forward radiation, which would then ensure the suppression of non-global, including super-leading, logarithms.

In the following section, we study the definition and kinematics of rapidity gap processes and review the relevant factorization procedure. Here, we introduce the energy flow defined in Ref. [10], and define the gap fraction. After studying the gap fraction in terms of energy flow, we study its relation to color flow at short distances in Secs. 3 and 4. We argue that the gap fraction exposes the pattern of soft gluon radiation, depending on the color SU(3) gauge content of the resonance in  $q\bar{q}(gg) \rightarrow Z'/G \rightarrow Q\bar{Q}$ . In Sec. 5, the gap fraction for heavy quark pair production induced by a heavy spin-1 resonance is studied. Finally, in Sec. 6, we apply our formalism for a study of spin-0 or 2 resonance particles associated with different partonic processes.

## 2 Heavy Quark Pair Rapidity Gap Cross Sections

### 2.1 Definitions

In this paper, we will focus on rapidity gap cross sections for heavy quark pair production through a new physics particle resonance denoted by  $V'(M, sp)$  of mass  $M$  and spin  $sp$ . The partonic scattering process for proton and (anti)-proton collisions, creating  $s$ -channel resonance  $V'$ , is

$$f : f_1(p_1) + f_2(p_2) \rightarrow V'(M, sp) \rightarrow Q(p_a) + \bar{Q}(p_b) + \Omega_{gap}(Q_c) + X, \quad (1)$$

for the production of a heavy quark pair at fixed rapidity difference,  $\Delta\eta = \eta_a - \eta_b$ . Here the  $f_i$  refer to partons that participate in the collision, and we have labeled process (1) “f”. We sum inclusively over final states, while measuring the energy flow,  $Q_c$ , into the rapidity region,  $\Omega_{gap}$ , in Eq. (1). The transverse momentum  $p_T$  of a parton  $Q(p_a)$  or  $\bar{Q}(p_b)$  of mass  $m_Q$  in Eq. (1) is related to the rapidity difference  $\Delta\eta$  according to

$$p_T = \sqrt{\frac{M^2}{4 \cosh^2 \frac{\Delta\eta}{2}} - m_Q^2}. \quad (2)$$

As discussed in the introduction, we may expect different patterns of radiation from intermediate resonances if they are distinguished by different gauge content.

The geometry for the gap at a collider is presented schematically in Fig. 1, where the gap region is determined by rapidity range  $Y$ . The factorization that we will discuss in Sec. 2.2 enables us to work perturbatively. The partonic cross section at leading order for process (1) involves five external particles. The kinematics of this analysis are described in the Appendix.

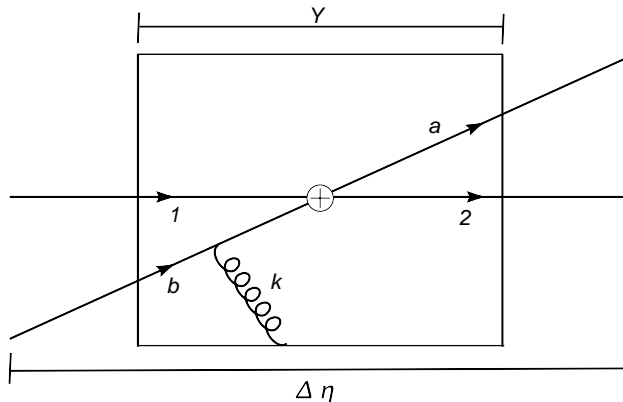


Figure 1: Light to heavy process with gluon radiation of momentum  $k^\mu$  into a rapidity gap. The figure describes  $q\bar{q} \rightarrow Q\bar{Q}$  process.  $\Delta\eta$  is the rapidity difference of a heavy quark pair,  $Q(p_a)$  and  $\bar{Q}(p_b)$ , and  $Y$  is the rapidity range of the gap region. 1 and 2 denote the initial partons while  $a$  and  $b$  denote the final partons.

## 2.2 Factorized and refactorized cross sections

The inclusive cross section for heavy quark pair production at rapidity difference  $\Delta\eta$  from a resonance at mass  $M$  with fixed energy flow  $Q_c$  is given in standard factorized form by

$$\frac{d\sigma_{AB}}{d\Delta\eta dQ_c} = \sum_{f_1, f_2} \int dx_1 dx_2 \phi_{f_1/A}(x_1, \mu_F) \phi_{f_2/B}(x_2, \mu_F) \frac{d\hat{\sigma}^{(f)}}{d\Delta\eta dQ_c}. \quad (3)$$

Here  $\phi_{f_1/A}$  and  $\phi_{f_2/B}$  are parton distribution functions (PDFs), evaluated at the factorization scale  $\mu_F$ . Below, we use the scale  $\mu_F = p_T$ , the transverse momentum  $p_T$  in Eq. (2). The partonic scattering cross section  $d\hat{\sigma}^{(f)}/d\Delta\eta dQ_c$  can be expanded in  $\alpha_s$ , starting from the

lowest order (LO) Born cross section

$$\frac{d\hat{\sigma}^{(f)}}{d\Delta\eta dQ_c} = \frac{d\hat{\sigma}^{(f,LO)}}{d\Delta\eta} \delta(Q_c) + \dots, \quad (4)$$

where corrections may include potentially large logarithms of  $p_T/Q_c$ . We recall that the index  $f$  denotes the partonic process in Eq. (1). Following Ref. [11], we consider the partonic cross sections integrated over the transverse energy,  $Q_c$ , radiated into a symmetric, central rapidity gap region,  $Y$  in Fig. 1, up to a fixed value  $Q_0$ ,

$$\frac{d\hat{\sigma}^{(f)}(M, m_Q, Q_0, \mu_F, \Delta\eta, Y, \alpha_s(\mu_F))}{d\Delta\eta} = \int_0^{Q_0} dQ_c \frac{d\hat{\sigma}^{(f)}(M, m_Q, Q_c, \mu_F, \Delta\eta, Y, \alpha_s(\mu_F))}{d\Delta\eta dQ_c}. \quad (5)$$

When Eq. (5) is divided by the total cross section, the ratio can be interpreted as the probability for heavy quark pair production with soft gluon radiation into the gap region up to energy flow  $Q_0$ . For simplicity of notation, we keep dependence on the resonance width  $\Gamma$  implicit but recall that we treat  $\Gamma/M$  as a number of order unity.

The partonic cross sections of Eq. (5) can be further refactorized into a hard scattering matrix  $H_{IL}^{(f)}$  and a soft matrix  $S_{LI}^{(f)}$ ,

$$\begin{aligned} \frac{d\hat{\sigma}^{(f)}}{d\Delta\eta}(M, m_Q, Q_0, \mu_F, \Delta\eta, Y, \alpha_s(\mu_F)) &= \sum_{L,I} H_{IL}^{(f)}(M, m_Q, \mu_F, \mu, \Delta\eta, \alpha_s(\mu)) \\ &\times S_{LI}^{(f)}\left(\Delta\eta, Y, \frac{Q_0}{\mu}, \alpha_s(\mu), m_Q\right), \end{aligned} \quad (6)$$

where matrix  $H_{IL}^{(f)}$  represents interactions at short distances, independent of soft gluon radiation, and contains the dynamics of resonance  $V'(M, sp)$ . Here we have introduced a new refactorization scale  $\mu$ . The soft function  $S_{LI}^{(f)}$  describes the radiation of soft gluons up to the scale  $Q_0$ , which decouples from the dynamics of the hard scattering. The soft function is written in terms of products of path-ordered exponentials,  $w_L^{(f)}(x)_{\{b_i\}}$ , of the gluon field as [11],

$$S_{LI}^{(f)} = \int_0^{Q_0} dQ'_c \sum_n \sum_{\{b_i\}} \delta(Q_0^{(n)} - Q'_c) \langle 0 | \bar{T}[(w_L^{(f)}(0))_{\{b_i\}}^\dagger] | n \rangle \langle n | T[(w_I^{(f)}(0))_{\{b_i\}}] | 0 \rangle, \quad (7)$$

where we sum over all states  $n$  whose transverse energy flow into the gap is restricted to equal  $Q'_c$  and where color tensors labeled by  $L$  and  $I$  account for the color flow at the hard scattering. Eikonal multipoint operators,  $(w_L^{(f)}(x))_{\{b_i\}}$ , with color indices  $\{b_i\}$  are written as

products of ordered exponentials, tied together by color tensors,  $c_L$ ,

$$(w_L^{(f)}(x))_{\{b_i\}} = \sum_{\{d_i\}} \Phi_{\beta_b}^{(f_b)}(\infty, 0; x)_{b_b, d_b} \Phi_{\beta_a}^{(f_a)}(\infty, 0; x)_{b_a, d_a} \\ \times (c_L^{(f)})_{d_b, d_a; d_1, d_2} \Phi_{\beta_1}^{(f_1)}(0, -\infty; x)_{d_1, b_1} \Phi_{\beta_2}^{(f_2)}(0, -\infty; x)_{d_2, b_2}, \quad (8)$$

where the non-Abelian path-ordered phase operators (Wilson lines),  $\Phi_\beta^{(f)}$ , are given by

$$\Phi_\beta^{(f)}(\infty, 0; x) = P \exp \left[ -ig \int_0^\infty d\lambda \beta \cdot A^{(f)}(\lambda \beta + x) \right]. \quad (9)$$

Here,  $\beta$  is a four-velocity, and the vector potentials  $A^{(f)}$  are in the color representation appropriate to flavor  $f$ . At the tree level, Eq. (7) reduces to the trace of the product of color tensors.

The product of hard and soft functions in Eq. (6) is independent of the refactorization scale,  $\mu$ . From this, we easily derive for  $S_{LI}^{(f)}$  the evolution equation [2]

$$\left( \mu \frac{\partial}{\partial \mu} + \beta(g_s) \frac{\partial}{\partial g_s} \right) S_{LI}^{(f)} = -(\Gamma_S^{(f)})_{LJ}^\dagger S_{JI}^{(f)} - S_{LJ}^{(f)} (\Gamma_S^{(f)})_{JI}, \quad (10)$$

in terms of a matrix of anomalous dimensions,  $(\Gamma_S^{(f)})_{JI}$ . The matrix  $\Gamma_S^{(f)}(\Delta\eta, Y, \rho)$  depends on kinematics, including the geometric information of the gap region and the heavy quark mass. Solving this equation will enable us to resum the leading logarithms of the soft scale  $Q_0$ . In heavy quark pair production, dependence on quark mass and the partonic center of mass energy  $M$  in soft functions will always appear through the parameter  $\rho$ , given by

$$\rho \equiv \sqrt{1 + \left( \frac{m_Q}{p_T} \right)^2} = \frac{1}{\sqrt{1 - 4 \frac{m_Q^2}{M^2} \cosh^2 \frac{\Delta\eta}{2}}}. \quad (11)$$

We will find that the soft function depends on the velocities  $\beta_i$  only through  $\Delta\eta$  and  $\rho$ .

To obtain the solution to Eq. (10), we treat above equation in a basis that diagonalizes  $\Gamma_S^{(f)}$ ,

$$(\Gamma_S^{(f)}(\Delta\eta, Y, \rho))_{\gamma\beta} \equiv \lambda_\beta^{(f)}(\Delta\eta, Y, \rho) \delta_{\gamma\beta} \\ = (R^{(f)})_{\gamma I} (\Gamma_S^{(f)}(\Delta\eta, Y, \rho))_{IJ} (R^{(f)})_{J\beta}^{-1}, \quad (12)$$

where the eigenvalues  $\lambda_\beta^{(f)}$  are given by a series in  $\alpha_s$ ,

$$\lambda_\beta^{(f)}(\Delta\eta, Y, \rho) = \frac{\alpha_s}{\pi} \lambda_\beta^{(f,1)}(\Delta\eta, Y, \rho) + \dots. \quad (13)$$



We can transform the soft and hard matrices in the diagonalized basis

$$\begin{aligned} S_{\gamma\beta}^{(\text{f})} &= [((R^{(\text{f})})^{-1})^\dagger]_{\gamma L} S_{LK}^{(\text{f})} [(R^{(\text{f})})^{-1}]_{K\beta}, \\ H_{\gamma\beta}^{(\text{f})} &= [R^{(\text{f})}]_{\gamma K} H_{KL}^{(\text{f})} [R^{(\text{f})}{}^\dagger]_{L\beta}. \end{aligned} \quad (14)$$

This change of basis uses the transformation matrix  $[(R^{(\text{f})})^{-1}]_{K\beta} = (e_\beta)_K$ , where  $e_\beta$  are eigenvectors of the soft anomalous dimension matrix.

The solution to Eq. (10) gives the dependence of  $S^{(\text{f})}$  on the ratio  $\mu/Q_0$ ,

$$\begin{aligned} S_{\gamma\beta}^{(\text{f})} \left( \Delta\eta, Y, \frac{Q_0}{\mu}, \alpha_s(\mu), \rho \right) &= S_{\gamma\beta}^{(\text{f})}(\Delta\eta, Y, 1, \alpha_s(Q_0), \rho) \exp \left[ -E_{\gamma\beta}^{(\text{f})} \int_{Q_0}^{\mu} \frac{d\mu'}{\mu'} \left( \frac{\beta_0}{2\pi} \alpha_s(\mu') \right) \right] \\ &= S_{\gamma\beta}^{(\text{f})}(\Delta\eta, Y, 1, \alpha_s(Q_0), \rho) \left[ \ln \left( \frac{Q_0}{\Lambda} \right) \right]^{E_{\gamma\beta}^{(\text{f})}} \left[ \ln \left( \frac{\mu}{\Lambda} \right) \right]^{-E_{\gamma\beta}^{(\text{f})}}. \end{aligned} \quad (15)$$

We will choose below  $\mu$  and  $\mu_F$  to be the hard scale  $p_T$  for use in the refactorized partonic cross section (6). In Eq. (15) the exponents  $E_{\alpha\beta}^{(\text{f})}$  are given in terms of sums of the eigenvalues of  $\Gamma_S$  by

$$E_{\gamma\beta}^{(\text{f})}(\Delta\eta, Y, \rho) = \frac{2}{\beta_0} [\lambda_{\gamma}^{(\text{f},1)*}(\Delta\eta, Y, \rho) + \lambda_{\beta}^{(\text{f},1)}(\Delta\eta, Y, \rho)], \quad (16)$$

where  $\beta_0$  is the lowest-order coefficient in the expansion of the QCD beta function,  $\beta_0 = (11N_c - 2n_f)/3$ , for  $N_c$  colors and  $n_f$  quark flavors. Equation (16) shows that the diagonal exponents,  $E_{\alpha\alpha}^{(\text{f})}$ , are real. In the second form of Eq. (15), we have used the one-loop QCD running coupling,

$$\alpha_s(\mu) = \frac{2\pi}{\beta_0 \ln(\mu/\Lambda)}. \quad (17)$$

Combining Eqs. (6) and (15), the partonic cross section, valid to leading logarithm, is then

$$\frac{d\hat{\sigma}^{(\text{f})}}{d\Delta\eta} = \sum_{\beta, \gamma} H_{\beta\gamma}^{(\text{f}, LO)}(M, m_Q, \Delta\eta, \alpha_s(p_T)) S_{\gamma\beta}^{(\text{f}, 0)} \left[ \ln \left( \frac{Q_0}{\Lambda} \right) \right]^{E_{\gamma\beta}^{(\text{f})}} \left[ \ln \left( \frac{p_T}{\Lambda} \right) \right]^{-E_{\gamma\beta}^{(\text{f})}}. \quad (18)$$

In the following section, we will use Eq. (18) to evaluate the gap fraction.

## 2.3 The gap fraction

We define the gap fraction  $f_{\text{gap}}$  as the ratio of the number of events for heavy quark pair production with a specified rapidity gap to the total number of the pair production events.

A gap event was originally identified experimentally by the lack of particle multiplicity in the interjet region [5, 8]. In that case, the multiplicity is determined from the number of calorimeter cells which measure energy deposition above a threshold. A gap event is then defined by the absence of such cells in the rapidity region. Our formulation of the problem is in terms of the transverse energy flow,  $Q_c$ , of hadronic radiation carried by the particles [10]. We introduce a variable, energy “gap threshold”  $Q_0$ , which is different in principle from the experimental calorimeter threshold, and identify a gap event from the condition of interjet radiation less than  $Q_0$ . Then, to get the partonic gap cross section, we evaluate Eq. (5) at the value  $Q_0$  for the maximum of interjet energy flow  $Q_c$ . The resummed result is given by Eq. (18). We note that values of  $Q_0$  at the order of the hard scale  $p_T$  would violate the requirement of factorization, since the emission into the gap region would not be soft any more.

To define the gap fraction, we approximate the total cross sections from the LO (Born) partonic cross section, related to Eq. (6)

$$\frac{d\hat{\sigma}^{(\text{f},LO)}}{d\Delta\eta} = \sum_{\beta,\gamma} H_{\beta\gamma}^{(\text{f},LO)}(M, m_Q, \Delta\eta, \alpha_s(p_T)) S_{\gamma\beta}^{(\text{f},0)}. \quad (19)$$

We may consider the LO and the gap differential partonic cross sections with respect to  $M$  and  $\eta_{V'} = \frac{1}{2} \ln \frac{x_1}{x_2}$ , given for a resonance by, respectively,

$$\begin{aligned} \frac{d\hat{\sigma}^{(\text{f},LO)}(M, m_Q, \Delta\eta, \alpha_s(p_T), Y)}{d\Delta\eta dM^2 d\eta_{V'}} &= \frac{d\hat{\sigma}^{(\text{f},LO)}}{d\Delta\eta} \delta(M^2 - x_1 x_2 S) \delta\left(\eta_{V'} - \frac{1}{2} \ln \frac{x_1}{x_2}\right), \\ \frac{d\hat{\sigma}^{(\text{f})}(M, m_Q, Q_0, \Delta\eta, \alpha_s(p_T), Y)}{d\Delta\eta dM^2 d\eta_{V'}} &= \frac{d\hat{\sigma}^{(\text{f})}}{d\Delta\eta} \delta(M^2 - x_1 x_2 S) \delta\left(\eta_{V'} - \frac{1}{2} \ln \frac{x_1}{x_2}\right), \end{aligned} \quad (20)$$

which are distinguished by the argument  $Q_0$  in the latter, and where  $S$  is the hadronic center of mass energy. Here, the differential with respect to  $\eta_{V'}$  corresponds to fixing the center of mass rapidity of the final-state pair in the lab frame. We emphasize that the above condition does not change the description of soft QCD radiation in the soft functions, which depend on the rapidity difference  $\Delta\eta$ .

We now define the gap fraction at leading order in terms of Eqs. (18), (19) and (20), by

$$f_{gap}^{(LO)} = \frac{\sum_{f_1, f_2} \int dx_1 dx_2 \phi_{f_1/A}(x_1) \phi_{f_2/B}(x_2) \frac{d\hat{\sigma}^{(\text{f})}(M, m_Q, Q_0, \Delta\eta, \alpha_s(p_T), Y)}{d\Delta\eta dM^2 d\eta_{V'}}}{\sum_{f_1, f_2} \int dx_1 dx_2 \phi_{f_1/A}(x_1) \phi_{f_2/B}(x_2) \frac{d\hat{\sigma}^{(\text{f},LO)}(M, m_Q, \Delta\eta, \alpha_s(p_T), Y)}{d\Delta\eta dM^2 d\eta_{V'}}}. \quad (21)$$

An advantage of using the differential partonic cross sections (20) to obtain the gap fraction becomes clear when there is only one partonic initial state for a resonance process. The gap fraction at leading order in Eq. (21) for a single partonic channel process is given by

$$f_{gap}^{(LO)}(M, m_Q, Q_0, \Delta\eta, \alpha_s(p_T), Y, \eta_{V'}) = \frac{\frac{d\hat{\sigma}^{(\dagger)}(M, m_Q, Q_0, \Delta\eta, \alpha_s(p_T), Y)}{d\Delta\eta}}{\frac{d\hat{\sigma}^{(\dagger, LO)}(M, m_Q, \Delta\eta, \alpha_s(p_T), Y)}{d\Delta\eta}}, \quad (22)$$

where the PDFs cancel in the ratios of the gap fraction in this case.

### 3 Massive Gap Soft Anomalous Dimension Matrices

The one-loop soft anomalous dimension matrix,  $\Gamma_S$ , for a rapidity gap process is calculated from the mismatch between real and virtual corrections, generated by imposing a rapidity gap. The soft function is calculated by taking single ultraviolet pole parts from virtual and real corrections, which we will label as  $\omega_{V(ij)}$  and  $\omega_{R(ij)}$ , respectively. The real part,  $\omega_{R(ij)}$ , comes with a phase space integral outside the gap, where it cancels  $\omega_{V(ij)}$ . The coefficient of the pole results from the phase space integration inside the rapidity gap region. Here, the single ultraviolet pole arises from the limitation on the energy integration of soft gluons.

In practice, following [11], we construct the gap soft anomalous dimension matrix from a set of integrals,  $\omega_{(ij)}$ ,

$$\gamma_{S(ij)}^{(1)} = \frac{\omega_{(ij)}(-2\varepsilon)}{(\alpha_s/\pi)}, \quad (23)$$

where we use dimensional regularization, with  $D = 4 - 2\varepsilon$ . The indices  $i$  and  $j$  label partons of momenta  $p_i$  and  $p_j$ , and the  $\omega_{(ij)}$  are defined by

$$\begin{aligned} \omega_{(ij)} &= \omega_{V(ij)} + \omega_{R(ij)} \\ &= -(4\pi\alpha_s)\delta_i\delta_j\Delta_i\Delta_j \int_{P.P.} \frac{d^D k}{(2\pi)^{D-1}} \delta_+(k^2) \Theta(\vec{k}) \frac{(p_i \cdot p_j)}{(p_i \cdot k)(p_j \cdot k)} \\ &\quad + \delta_i\delta_j\Delta_i\Delta_j \frac{\alpha_s}{2\pi} \frac{i\pi}{2\varepsilon} (1 - \delta_i\delta_j). \end{aligned} \quad (24)$$

Here the subscript  $P.P.$  indicates that the integral is defined by its ultraviolet pole part. We also define  $\delta_i = 1(-1)$  for momentum  $k$  flowing in the same (opposite) direction as the momentum flow of line  $i$ , and  $\Delta_i = 1(-1)$  for  $i$  a quark (antiquark) line. The function  $\Theta(\vec{k}) = 1$  when the vector  $\vec{k}$  is directed into a rapidity gap. Equation (24) describes the incomplete

cancellation between real and virtual gluons from the integration over the geometric phase space of the gap region. Only the part of the phase integration inside the gap survives, and contributes to the soft anomalous dimension matrix for the process.

We express the above integrals in terms of transverse momentum, rapidity, and azimuthal angle coordinates, with the help of the kinematics described in the Appendix, and use the relations

$$\begin{aligned}\int_{P.P.} d^D k \delta_+(k^2) &= \int_{P.P.} \frac{k_T^{D-3}}{2} dk_T dy d\phi, \\ \int_{P.P.} \frac{dk_T}{k_T^{1+2\varepsilon}} &= \frac{1}{2\varepsilon}.\end{aligned}\tag{25}$$

In these terms, the  $\omega_{(ij)}$  become

$$\omega_{(ij)} = \left(\frac{\alpha_s}{\pi}\right) \left( -\delta_i \delta_j \Delta_i \Delta_j \frac{1}{2} \frac{1}{2\varepsilon} \int \frac{dy d\phi}{2\pi} \Theta(\vec{k}) \Omega_{ij} + \delta_i \delta_j \Delta_i \Delta_j \frac{i\pi}{2\varepsilon} \frac{(1 - \delta_i \delta_j)}{2} \right), \tag{26}$$

where we define  $\Omega_{ij}$  as

$$\Omega_{ij} = \frac{(p_i \cdot p_j) k_T^2}{(p_i \cdot k)(p_j \cdot k)}.\tag{27}$$

In these coordinates, the  $\Omega_{ij}$  are given by

$$\begin{aligned}\Omega_{12} &= 2, \\ \Omega_{ab} &= \frac{\rho^2 \cosh \Delta\eta + 1}{(\rho \cosh(\frac{\Delta\eta}{2} - y) - \cosh \phi) (\rho \cosh(\frac{\Delta\eta}{2} + y) + \cosh \phi)}, \\ \Omega_{1a} &= \frac{\rho e^{-(\frac{\Delta\eta}{2} - y)}}{(\rho \cosh(\frac{\Delta\eta}{2} - y) - \cosh \phi)}, \\ \Omega_{1b} &= \frac{\rho e^{(\frac{\Delta\eta}{2} + y)}}{(\rho \cosh(\frac{\Delta\eta}{2} + y) + \cosh \phi)}, \\ \Omega_{2a} &= \frac{\rho e^{(\frac{\Delta\eta}{2} - y)}}{(\rho \cosh(\frac{\Delta\eta}{2} - y) - \cosh \phi)}, \\ \Omega_{2b} &= \frac{\rho e^{-(\frac{\Delta\eta}{2} + y)}}{(\rho \cosh(\frac{\Delta\eta}{2} + y) + \cosh \phi)}.\end{aligned}\tag{28}$$

We recall that indices 1 and 2 are for initial-state partons, and  $a$  and  $b$  for final-state partons, as described in Eq. (1). The parameter  $\rho$  has been defined in Eq. (11), and is always larger than one for massive partons and equal to one for the massless case. We will see that

all the results we derive here go back to the previous calculation for massless dijet events,  $\rho = 1$  [10, 12].

For complete integrations over the rapidity gap geometry, it is convenient to integrate  $\Omega_{ij}$  over an azimuthal angle  $\phi$  first. It is then straightforward to evaluate rapidity integrals over a gap region  $-Y/2$  to  $Y/2$ . The final expressions for the  $\gamma_S^{(1)}(ij)$  of Eq. (23) are then

$$\begin{aligned}
\gamma_S^{(1)}(12) &= Y - i\pi, \\
\gamma_S^{(1)}(ab) &= -i\pi + \frac{\rho^2 \cosh \Delta\eta + 1}{2\rho \cosh(\frac{\Delta\eta}{2}) \sqrt{1 + \rho^2 \sinh^2(\frac{\Delta\eta}{2})}} \\
&\quad \times \ln \left( \frac{\rho^2 \cosh(\frac{\Delta\eta+Y}{2}) \sinh(\frac{\Delta\eta}{2}) + \sinh(\frac{Y}{2}) + \sqrt{(\rho^2 \sinh^2(\frac{\Delta\eta}{2}) + 1)(\rho^2 \cosh^2(\frac{\Delta\eta+Y}{2}) - 1)}}{\rho^2 \cosh(\frac{\Delta\eta-Y}{2}) \sinh(\frac{\Delta\eta}{2}) - \sinh(\frac{Y}{2}) + \sqrt{(\rho^2 \sinh^2(\frac{\Delta\eta}{2}) + 1)(\rho^2 \cosh^2(\frac{\Delta\eta-Y}{2}) - 1)}} \right), \\
\gamma_S^{(1)}(1a) &= \frac{1}{4} \ln \left( \frac{2\rho \left( \rho \cosh^2(\frac{\Delta\eta+Y}{2}) + \sinh(\frac{\Delta\eta+Y}{2}) \sqrt{\rho^2 \cosh^2(\frac{\Delta\eta+Y}{2}) - 1} \right) - (\rho^2 + 1)}{2\rho \left( \rho \cosh^2(\frac{\Delta\eta-Y}{2}) + \sinh(\frac{\Delta\eta-Y}{2}) \sqrt{\rho^2 \cosh^2(\frac{\Delta\eta-Y}{2}) - 1} \right) - (\rho^2 + 1)} \right) \\
&\quad - \frac{1}{2} \ln \left( \frac{\rho \cosh(\frac{\Delta\eta+Y}{2}) + \sqrt{\rho^2 \cosh^2(\frac{\Delta\eta+Y}{2}) - 1}}{\rho \cosh(\frac{\Delta\eta-Y}{2}) + \sqrt{\rho^2 \cosh^2(\frac{\Delta\eta-Y}{2}) - 1}} \right), \\
\gamma_S^{(1)}(1b) &= -\frac{1}{4} \ln \left( \frac{2\rho \left( \rho \cosh^2(\frac{\Delta\eta+Y}{2}) + \sinh(\frac{\Delta\eta+Y}{2}) \sqrt{\rho^2 \cosh^2(\frac{\Delta\eta+Y}{2}) - 1} \right) - (\rho^2 + 1)}{2\rho \left( \rho \cosh^2(\frac{\Delta\eta-Y}{2}) + \sinh(\frac{\Delta\eta-Y}{2}) \sqrt{\rho^2 \cosh^2(\frac{\Delta\eta-Y}{2}) - 1} \right) - (\rho^2 + 1)} \right) \\
&\quad - \frac{1}{2} \ln \left( \frac{\rho \cosh(\frac{\Delta\eta+Y}{2}) + \sqrt{\rho^2 \cosh^2(\frac{\Delta\eta+Y}{2}) - 1}}{\rho \cosh(\frac{\Delta\eta-Y}{2}) + \sqrt{\rho^2 \cosh^2(\frac{\Delta\eta-Y}{2}) - 1}} \right), \\
\gamma_S^{(1)}(2a) &= \gamma_S^{(1)}(1b), \\
\gamma_S^{(1)}(2b) &= \gamma_S^{(1)}(1a). \tag{29}
\end{aligned}$$

We take the massless limit,  $\rho = 1$ , in Eq. (29) to cross-check these results with the previous

calculation for massless dijet events, and find [12]

$$\begin{aligned}
\gamma_{S(12)}^{(1)} &= Y - i\pi, \\
\gamma_{S(ab)}^{(1)} &= \ln \left( \frac{\sinh \left( \frac{\Delta\eta+Y}{2} \right)}{\sinh \left( \frac{\Delta\eta-Y}{2} \right)} \right) - i\pi, \\
\gamma_{S(1a)}^{(1)} &= \gamma_{S(2b)}^{(1)} = \frac{1}{2} \left( \ln \left( \frac{\sinh \left( \frac{\Delta\eta+Y}{2} \right)}{\sinh \left( \frac{\Delta\eta-Y}{2} \right)} \right) - Y \right), \\
\gamma_{S(1b)}^{(1)} &= \gamma_{S(2a)}^{(1)} = -\frac{1}{2} \left( \ln \left( \frac{\sinh \left( \frac{\Delta\eta+Y}{2} \right)}{\sinh \left( \frac{\Delta\eta-Y}{2} \right)} \right) + Y \right).
\end{aligned} \tag{30}$$

We can now construct the soft anomalous dimension matrices which depend on the color basis. We use an  $s$ -channel singlet-octet basis [51] for quark-antiquark annihilation to a heavy quark pair,

$$c_{singlet} = c_1, \quad c_{octet} = -\frac{1}{2N_c}c_1 + \frac{c_2}{2}, \tag{31}$$

where  $c_1$  and  $c_2$  are color tensor basis for singlet exchange in the  $s$  and  $t$  channels,

$$(c_1)_{\{r_i\}} = \delta_{r_1 r_2} \delta_{r_a r_b}, \quad (c_2)_{\{r_i\}} = \delta_{r_1 r_a} \delta_{r_2 r_b}. \tag{32}$$

Here, we denote by  $r_i$  the color index associated with the incoming or outgoing parton  $i$ . The lowest-order soft matrix is the trace of the color basis,  $S_{LI}^{(f,0)} = \text{Tr}(c_L^\dagger c_I)$ , given in singlet-octet basis by

$$S^{(f,0)} = \begin{pmatrix} N_c^2 & 0 \\ 0 & \frac{1}{4}(N_c^2 - 1) \end{pmatrix}, \tag{33}$$

which will be used in the resummed cross sections, Eq. (18).

To construct the soft anomalous dimension matrix in the color basis (31), we rewrite the various one-loop diagrams, using the identity shown in Fig. 2:

$$(T_F^a)_{ji}(T_F^a)_{kl} = \frac{1}{2} \left( \delta_{ki} \delta_{jl} - \frac{1}{N_c} \delta_{ji} \delta_{kl} \right), \tag{34}$$

where the  $T_F^a$ 's are the generators of  $\text{SU}(N_c)$  in the fundamental representation. In the basis of Eq. (31) for the process  $q\bar{q} \rightarrow Q\bar{Q}$ , we derive in this way the soft anomalous dimension matrix in terms of the integrals  $\gamma_{S(ij)}^{(1)}$  in Eq. (29),

$$\Gamma_S^{(1)(q\bar{q} \rightarrow Q\bar{Q})} = \begin{pmatrix} C_F \alpha & \frac{C_F}{2N_c} (\chi + \tau) \\ \chi + \tau & C_F \chi - \frac{1}{2N_c} (2\tau + \alpha + \chi) \end{pmatrix}, \tag{35}$$

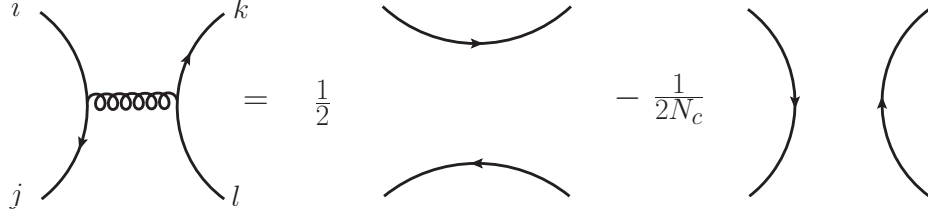


Figure 2: Color identity corresponding to Eq. (34).

where  $\alpha$ ,  $\chi$  and  $\tau$  are defined by

$$\begin{aligned}\alpha &\equiv \gamma_{S(12)}^{(1)} + \gamma_{S(ab)}^{(1)}, \\ \chi &\equiv \gamma_{S(1a)}^{(1)} + \gamma_{S(2b)}^{(1)}, \\ \tau &\equiv \gamma_{S(1b)}^{(1)} + \gamma_{S(2a)}^{(1)}.\end{aligned}\tag{36}$$

The eigenvectors of  $\Gamma_S^{(1)}$  in Eq. (35) may be chosen as

$$\begin{aligned}e_1 &= \begin{pmatrix} 1 \\ \frac{4N_c\xi}{\Delta_1 + \sqrt{\Delta_1^2 + 8C_F N_c \xi^2}} \end{pmatrix}, \\ e_2 &= \begin{pmatrix} \frac{\Delta_1 - \sqrt{\Delta_1^2 + 8C_F N_c \xi^2}}{4N_c\xi} \\ 1 \end{pmatrix},\end{aligned}\tag{37}$$

and the corresponding eigenvalues are given by

$$\begin{aligned}\lambda_1^{(f,1)} &= \frac{\Delta_2 + \sqrt{\Delta_1^2 + 8C_F N_c \xi^2}}{4N_c}, \\ \lambda_2^{(f,1)} &= \frac{\Delta_2 - \sqrt{\Delta_1^2 + 8C_F N_c \xi^2}}{4N_c},\end{aligned}\tag{38}$$

where we have defined

$$\begin{aligned}\Delta_1 &\equiv (\alpha + \chi + 2\tau) + 2C_F N_c(\alpha - \chi), \\ \Delta_2 &\equiv -(\alpha + \chi + 2\tau) + 2C_F N_c(\alpha + \chi), \\ \xi &\equiv (\tau + \chi).\end{aligned}\tag{39}$$

Finally, the transformation matrix  $R$  in Eq. (12), which diagonalizes the soft anomalous dimension matrix, is given from Eq. (37) by

$$(R^{(f)})_{J\beta}^{-1} = \begin{pmatrix} 1 & \frac{\Delta_1 - \sqrt{\Delta_1^2 + 8C_F N_c \xi^2}}{4N_c\xi} \\ \frac{4N_c\xi}{\Delta_1 + \sqrt{\Delta_1^2 + 8C_F N_c \xi^2}} & 1 \end{pmatrix}.\tag{40}$$

It was observed in Ref. [10] that for massless partons the above eigenvectors are independent of the rapidity difference  $\Delta\eta$ , and depend only on the rapidity gap range,  $Y$ . However, we find that this is not the case any more for massive quark pair production,  $\rho > 1$ . As an example, we take the values  $\Delta\eta = 2.5$  and  $\Delta\eta = 4$  at fixed  $m_Q = m_t$ ,  $M = 1.5$  TeV and  $Y = 1.5$ , and confirm a mild rapidity dependence of the eigenvectors,

$$\begin{aligned} e_1 &= \begin{pmatrix} 1 \\ -0.098 - 0.269i \end{pmatrix} \text{ for } \Delta\eta = 2.5, & e_1 &= \begin{pmatrix} 1 \\ -0.102 - 0.274i \end{pmatrix} \text{ for } \Delta\eta = 4, \\ e_2 &= \begin{pmatrix} 0.022 + 0.060i \\ 1 \end{pmatrix} \text{ for } \Delta\eta = 2.5, & e_2 &= \begin{pmatrix} 0.023 + 0.061i \\ 1 \end{pmatrix} \text{ for } \Delta\eta = 4. \end{aligned} \quad (41)$$

For these configurations, the first eigenvector,  $e_1$ , is close to a color singlet, while the second,  $e_2$ , is close to a color octet. Following the terminology in Ref. [10], we denote the eigenvectors,  $e_1$  and  $e_2$ , of  $\Gamma_S$  by “quasi-singlet” and “quasi-octet”, respectively.

We will see below that the process  $q\bar{q} \rightarrow Q\bar{Q}$  is the only relevant partonic channel involving a spin-1 particle resonance,  $V'(M, sp = 1)$ . For other resonances  $V'(M, sp \neq 1)$ , we can consider the gluon-induced partonic process

$$g(p_1) + g(p_2) \rightarrow V'(M, sp \neq 1) \rightarrow Q(p_a) + \bar{Q}(p_b) + \Omega_{\text{gap}}(Q_c). \quad (42)$$

To describe the color flow in the latter process, a suitable  $s$ -channel basis of color tensors has been defined in Ref. [11],

$$\begin{aligned} (c_1)_{\{r_i\}} &= \delta_{r_1 r_2} \delta_{r_a r_b}, \\ (c_2)_{\{r_i\}} &= d_{r_1 r_2 c} (T_F^c)_{r_a r_b}, \\ (c_3)_{\{r_i\}} &= i f_{r_1 r_2 c} (T_F^c)_{r_a r_b}, \end{aligned} \quad (43)$$

where  $c_1$  is again the  $s$ -channel singlet tensor, and  $c_2$  and  $c_3$  are the symmetric and anti-symmetric octet tensors, respectively. In this basis, the anomalous dimension matrix for the process  $gg \rightarrow Q\bar{Q}$  is found to be [12]

$$\Gamma_S^{(1)(gg \rightarrow Q\bar{Q})} = \begin{pmatrix} C_F \gamma_S^{(1)}(ab) + N_c \gamma_S^{(1)}(12) & 0 & \frac{1}{2}(\chi + \tau) \\ 0 & N_c \zeta & \frac{N_c}{4}(\chi + \tau) \\ \chi + \tau & \frac{N_c^2 - 4}{4N_c}(\chi + \tau) & N_c \zeta \end{pmatrix}, \quad (44)$$

where  $\zeta \equiv \frac{1}{4}(\chi - \tau) - \frac{1}{2N_c^2} \gamma_S^{(1)}(ab) + \frac{1}{2} \gamma_S^{(1)}(12)$ , and where  $\chi$  and  $\tau$  have been defined in Eq. (36). In analogy to Eq. (33), we derive the zeroth order soft matrix for this process in basis (43)



as

$$S^{(f,0)} = \begin{pmatrix} N_c(N_c^2 - 1) & 0 & 0 \\ 0 & \frac{(N_c^2 - 4)(N_c^2 - 1)}{2N_c} & 0 \\ 0 & 0 & \frac{N_c(N_c^2 - 1)}{2} \end{pmatrix}. \quad (45)$$

One may now find the corresponding eigenvalues and transformation matrices  $R^{(f)-1}$  for  $gg \rightarrow Q\bar{Q}$ . The results are too cumbersome to present here, but are straightforward to derive and evaluate numerically. In large  $N_c$  limit, however, the eigenvectors and the corresponding eigenvalues can be obtained readily, since Eq. (44) becomes

$$\Gamma_S^{(1)(gg \rightarrow Q\bar{Q})} \simeq N_c \begin{pmatrix} \frac{1}{2} \gamma_S^{(1)}{}_{(ab)} + \gamma_S^{(1)}{}_{(12)} & 0 & 0 \\ 0 & \zeta & \frac{1}{4}(\chi + \tau) \\ 0 & \frac{1}{4}(\chi + \tau) & \zeta \end{pmatrix}, \quad (46)$$

for large  $N_c$ . Normalized eigenvectors of  $\Gamma_S^{(gg \rightarrow Q\bar{Q})}$  in large  $N_c$  limit are then

$$e_1 = \begin{pmatrix} 1 \\ 0 \\ 0 \end{pmatrix}, \quad e_2 = \frac{1}{\sqrt{2}} \begin{pmatrix} 0 \\ 1 \\ 1 \end{pmatrix}, \quad e_3 = \frac{1}{\sqrt{2}} \begin{pmatrix} 0 \\ -1 \\ 1 \end{pmatrix}, \quad (47)$$

and the corresponding eigenvalues are given by

$$\begin{aligned} \lambda_1^{(f,1)} &= \left( \frac{1}{2} \gamma_S^{(1)}{}_{(ab)} + \gamma_S^{(1)}{}_{(12)} \right) N_c, \\ \lambda_2^{(f,1)} &= \left( \zeta + \frac{1}{4}(\chi + \tau) \right) N_c, \\ \lambda_3^{(f,1)} &= \left( \zeta - \frac{1}{4}(\chi + \tau) \right) N_c. \end{aligned} \quad (48)$$

We emphasize that, in Eq. (47),  $e_1$  is an exact color singlet and that  $e_2$  and  $e_3$  are octet basis vectors. We will not restrict ourselves the above approximation in following sections. We will see, however, in Sec. 6 that the explicit results of eigenvalues and eigenvectors for  $gg \rightarrow Q\bar{Q}$  in the kinematics and the gap geometry we study in this paper are close to the results of the large  $N_c$  limit.

The analysis in this section is based on wide resonances with  $\Gamma \sim M$  of decay width,  $\Gamma$ , and resonance mass,  $M$ . We note, however, that the energy scale  $\mu$  of gluon radiation

into a gap should be separated into two different regions, depending on the decay widths of heavy resonances. This may lead to different prescriptions for describing soft gluon radiation, depending on  $\mu$ . For gluon radiation at scale  $\mu$ , with  $Q_0 < \mu < \sqrt{\Gamma M}$ , the hard function can be treated as an effective vertex. This is the condition we have used for describing soft gluon radiation in this section, where we assume that the hard scale  $p_T$  is of the same order as  $\sqrt{\Gamma M}$ . For the case of gluon radiation in the range  $\sqrt{\Gamma M} < \mu < M$ , direct radiation from the resonance, which was not considered in this section, has to be included in the soft function. In addition to this, the contributions from soft gluon interactions between initial and final state partons are suppressed for both octet and singlet resonance processes if the hard scale falls into the regime  $\sqrt{\Gamma M} < \mu < M$ . In this paper, we concentrate on the case that  $\sqrt{\Gamma M}$  is of the order of  $p_T$ .<sup>1</sup> In general, the decay width of an octet resonance would be large enough to satisfy this condition. For example, a KK gluon above 1 TeV (as required by precision tests) has decay width of about  $M_G/6$  [27, 29] in basic RS models, and  $0.215M_G$  [32, 65] in RS models based on extended electroweak gauge symmetry with specific fermion charges and localization that explain the LEP anomaly of the forward-backward asymmetry for  $b$  quarks. Axigluons or universal colorons have decay width of about  $\alpha_s M_G$  [48], resulting in  $\sqrt{\Gamma M_G} \sim p_T$  where  $p_T$  is the hard scale we have used. On the other hand, the widths of singlet resonances are sensitive to the model parameters for the  $Z'$ . A  $Z'$  can be very narrow,  $\mathcal{O}(10^{-3}M_{Z'})$ , or very broad,  $\mathcal{O}(M_{Z'})$ , in both Topcolor  $Z'$  models [66] and in the Little Higgs models [67–70], depending on parameters such as the  $SU(2)_1 \otimes SU(2)_2$  mixing angle. In the following sections, our study will be based primarily on the broad widths of heavy resonances,  $Q_0 < \mu < \sqrt{\Gamma M}$ . We have observed that for narrow resonances we have to evolve  $\mu$  both from  $Q_0$  to  $\sqrt{\Gamma M}$  with the exponents we have obtained in this section and from  $\sqrt{\Gamma M}$  to the hard scale with a different analysis. We will discuss briefly how such a narrow singlet resonance can change our results at the end of Sec. 6.

## 4 Hard Functions

The remaining piece to complete constructing a partonic cross section in Eq. (6) is a hard function. Hard functions describe physics at the large momentum scale. In our study, the mechanism of new heavy particle resonances is thus contained in the hard functions,

---

<sup>1</sup> In principle, a hard scale for the specific model could be chosen as  $\sqrt{\Gamma M}$ , the minimum off-shellness of the resonance. The hard scale  $p_T$  is suitable in our study since we are interested in a model independent approach and since we consider broad resonances that satisfy  $\sqrt{\Gamma M} \sim p_T$  by assumption.

decoupled from soft QCD radiation. The direct radiation from an octet resonance can thus be neglected. In the previous section, we have constructed soft functions in the space of color flow at short distances. Thus, it is convenient to construct hard functions in the same basis. In Fig. 3, we represent several possible diagrams for the hard part, involving  $s$ -channel heavy resonances at lowest order. In the color basis (31), the corresponding hard functions for  $q\bar{q} \rightarrow G/Z' \rightarrow Q\bar{Q}$  in Figs. 3(a) and 3(b) are given by, respectively,

$$(H_G^{(\text{f},LO)})_{KL} = h_G(M, s, t, u) \begin{pmatrix} 0 & 0 \\ 0 & 1 \end{pmatrix}, \quad (49)$$

$$(H_{Z'}^{(\text{f},LO)})_{KL} = h_{Z'}(M, s, t, u) \begin{pmatrix} 1 & 0 \\ 0 & 0 \end{pmatrix}. \quad (50)$$

A hard function for  $gg \rightarrow G \rightarrow Q\bar{Q}$  in Fig. 3(c) such as a KK gluon resonance process [44,45] would take the form

$$(H_G'^{(\text{f},LO)})_{KL} = h'_G(M, s, t, u) \begin{pmatrix} 0 & 0 & 0 \\ 0 & 0 & 0 \\ 0 & 0 & 1 \end{pmatrix}, \quad (51)$$

and for  $gg \rightarrow Z' \rightarrow Q\bar{Q}$  in Fig. 3(d) a hard function is given by

$$(H_{Z'}'^{(\text{f},LO)})_{KL} = h'_{Z'}(M, s, t, u) \begin{pmatrix} 1 & 0 & 0 \\ 0 & 0 & 0 \\ 0 & 0 & 0 \end{pmatrix}, \quad (52)$$

in the color basis (43). The overall functions  $h_{G/Z'}(M, s, t, u)$  and  $h'_{G/Z'}(M, s, t, u)$  depend on hard scale kinematic variables,  $M$ ,  $s$ ,  $t$  and  $u$ , independent of the gap variables,  $Q_0$  and  $Y$ . We note that the spin of the particle  $V'$  limits possible partonic cross sections. Specifically, as noted in Refs. [71,72], the Landau-Yang theorem [73] forbids the creation of a massive state of total angular momentum  $J = 1$  from two massless spin-1 particles. Therefore, the gluon-induced production of a spin-1 massive state in Fig. 3(c) or 3(d) is not allowed if the spin of the resonance is one. Spin-0 singlet or octet resonances could arise, however, in split SUSY scenarios via  $gg$  annihilation. In such cases,  $gg \rightarrow G/Z'(sp = 0)$  could be the dominant production channel, giving hard functions of the forms, Eqs. (51) and (52). Also, spin-2 particles  $V'(sp = 2)$  such as gravitons and reggeons [74] could be created in  $s$ -channel resonances through  $gg \rightarrow V'(sp = 2) \rightarrow Q\bar{Q}$ , as well as  $q\bar{q} \rightarrow V'(sp = 2) \rightarrow Q\bar{Q}$ . The cross sections for resonances in these cases depend crucially on the model we study. For spin-1 resonance processes, we do not need to know specific coupling strength to the SM particles,

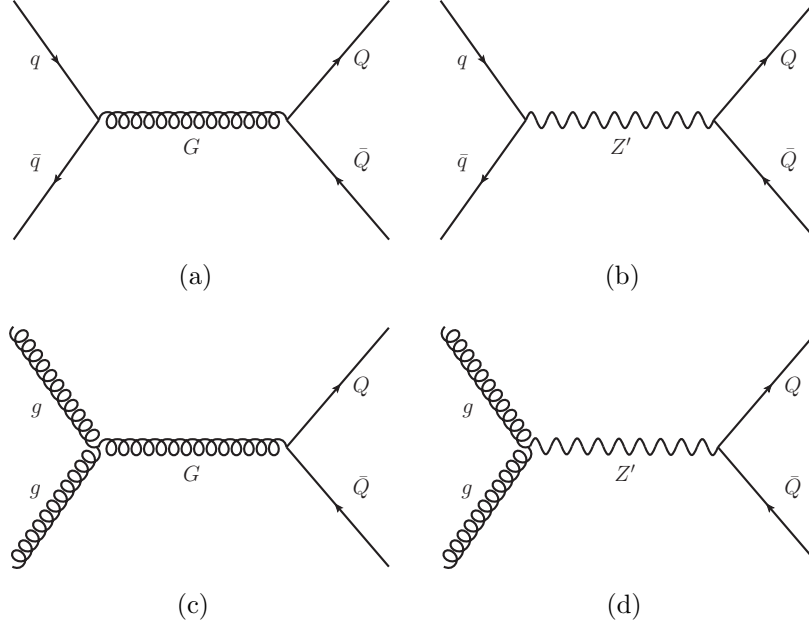


Figure 3: Figures (a)-(d) represent the resonance mechanisms for hard functions in Eqs. (49), (50), (51) and (52), respectively.

because spin-1  $G$  and  $Z'$  involve *only* the quark-induced partonic process,  $q\bar{q} \rightarrow G/Z' \rightarrow Q\bar{Q}$ . This simplifies the study of the gap fraction. According to the argument in Sec. 2.3, the gap fraction at leading logarithm results in the ratio of partonic cross sections (22), free from the PDFs that cancel in the ratios. Also,  $h_G$  or  $h_Z$  of the hard-scattering functions cancels in the ratios (22). We can thus study the gap fraction analytically.

In Sec. 6, we will discuss how gluon-induced resonances contribute to the gap fraction in massive spin-0 or 2 resonance processes. For a complete study of the gap fraction in this case, we should combine all the possible partonic processes that depend on the specific model. In addition to these, we must convolute the partonic level results with PDFs, following Eq. (3). We leave this study for a further project.

To obtain the partonic cross section in Eq. (18), hard functions in Eqs. (49), (50), (51), and (52) are transformed to  $(H^{(f,LO)})_{\gamma\beta}$  through Eq. (14) in the color basis that diagonalizes  $\Gamma_S^{(f)}$  in Eq. (12). We will study explicitly how partonic cross sections and gap fractions are evaluated in the following sections.

## 5 Gap Fractions for Spin-1 Resonances

From the previous sections, we have all the tools necessary for the evaluation of the partonic cross section in Eq. (18). As mentioned above, the main quantity we focus on is the gap fraction (21). For spin-1 resonances, we can limit ourselves to quark-induced resonances, shown in Figs. 3(a) and 3(b), following the argument in Sec. 4. The partonic cross section for heavy quark production via  $G$  or  $Z'$  resonances is

$$\frac{d\hat{\sigma}_{G/Z'}^{(f)}}{d\Delta\eta} = \sum_{\beta,\gamma} (H_{G/Z'}^{(f,LO)})_{\beta\gamma}(M, m_Q, \Delta\eta, \alpha_s(p_T)) S_{\gamma\beta}^{(f,0)} \left[ \frac{\ln\left(\frac{Q_0}{\Lambda}\right)}{\ln\left(\frac{p_T}{\Lambda}\right)} \right]^{E_{\gamma\beta}^{(f)}}, \quad (53)$$

where the  $(H_{G/Z'}^{(f,LO)})_{\beta\gamma}$  are hard functions written in the basis that diagonalizes the soft anomalous dimension matrix. We will implement Eq. (53) in numerical studies below. Following Eq. (14), to obtain  $(H_{G/Z'}^{(f,LO)})_{\beta\gamma}$ , we transform the hard functions in Eqs. (49) and (50), through matrix  $R$  given explicitly in Eq. (40). The soft matrix  $S_{\gamma\beta}^{(f,0)}$  is obtained by transforming Eq. (33) through the same matrix  $R$ . Finally, the exponents  $E_{\alpha\beta}^{(f)}$  that appear in the cross sections (53) are given by Eq. (16).

In Eq. (53), we observe that the  $Q_0$ -dependent factor,  $[\ln\left(\frac{Q_0}{\Lambda}\right) / \ln\left(\frac{p_T}{\Lambda}\right)]^{E_{\gamma\beta}^{(f)}}$ , is larger at fixed  $Q_0$  for smaller  $E_{\gamma\beta}^{(f)}$ , because  $[\ln\left(\frac{Q_0}{\Lambda}\right) / \ln\left(\frac{p_T}{\Lambda}\right)]$  is less than one for  $Q_0 < p_T$ . Note that we apply Eq. (53) only for  $Q_0 < p_T$ . A constraint for the maximum value of  $\Delta\eta$  is obtained from  $\rho$  in Eq. (11),

$$Y < \Delta\eta < 2 \cosh^{-1} \left( \frac{M}{2m_Q} \right). \quad (54)$$

Recall that the gap fraction measures the fraction of events for which the radiated transverse energy is less than or equal to the gap threshold  $Q_0$ . For any  $E_{\alpha\beta}^{(f)} > 0$ , the fraction vanishes for  $Q_0 = \Lambda$ , and approaches unity for  $Q_0 = p_T$ , where we choose  $\mu = p_T$  in numerical calculations. The soft anomalous dimension matrix for this analysis is given by Eq. (35). Representative numerical values of the real and imaginary parts of the eigenvalues are shown in Fig. 4 as a function of gap size  $Y$ . The corresponding exponents at fixed  $Y$  are shown in Fig. 5 as a function of  $\Delta\eta$ . Only the real parts enter the cross section. Imaginary parts are shown for completeness. Qualitatively, in Figs. 4 and 5, we see that the eigenvalues and the corresponding exponents are larger for larger  $Y$  and for smaller  $\Delta\eta$ . In Fig. 4, we observe that for  $Y$  of order unity,  $\text{Re}[\lambda_1]$  is much larger than  $\text{Re}[\lambda_2]$ , leading to  $E_{22}^{(f)} < 1 < E_{11}^{(f)}$ , as

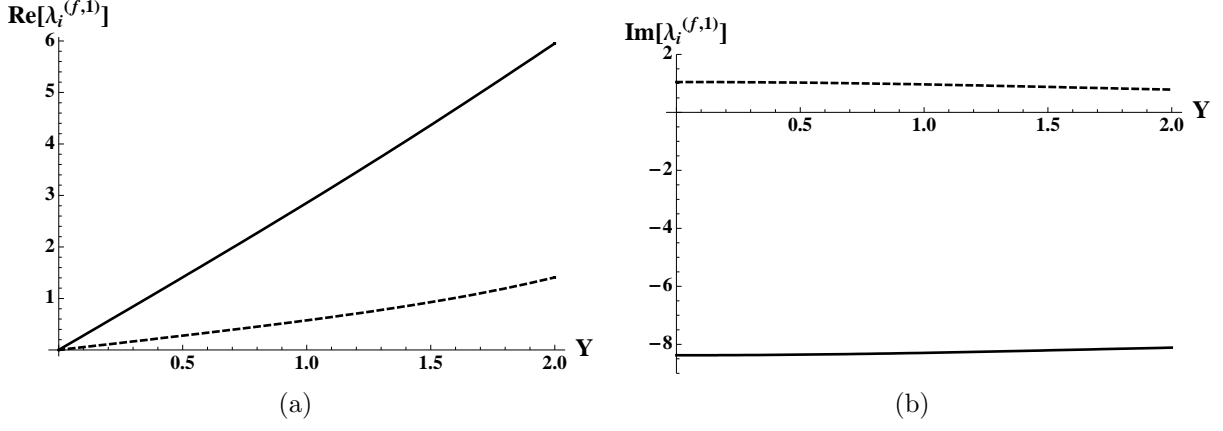


Figure 4: Plot of the real (a) and imaginary (b) parts of the eigenvalues of the soft anomalous dimension matrix in Eq. (35) for  $q\bar{q} \rightarrow Q\bar{Q}$ , as a function of  $Y$  for  $M = 1.5$  TeV,  $\Delta\eta = 2.5$  and  $m_Q = m_t$ . The solid line identifies the quasi-singlet eigenvalue,  $\lambda_1^{(f,1)}$ , the dashed line, quasi-octet,  $\lambda_2^{(f,1)}$ , in Eq. (37).

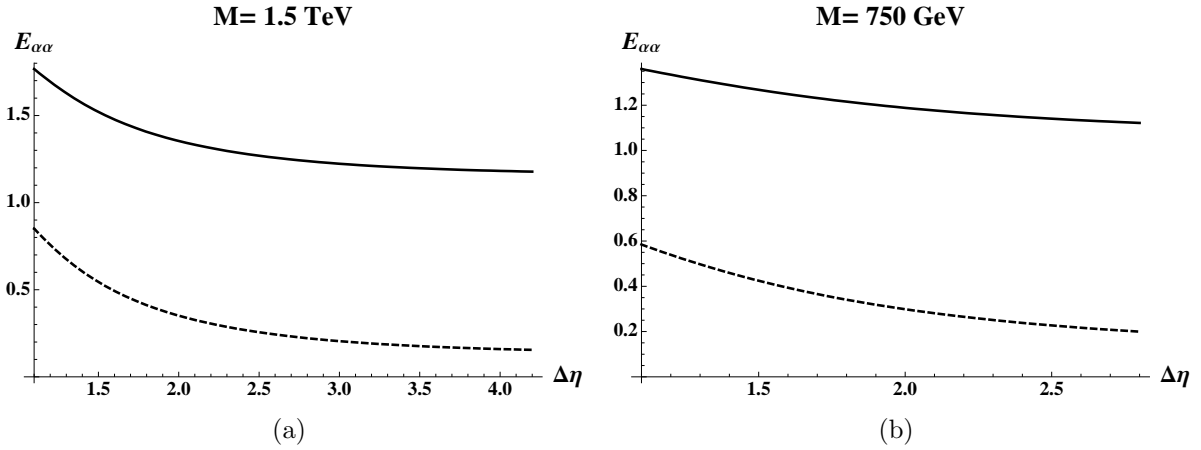


Figure 5: Plot of the exponents,  $E_{\alpha\alpha}^{(f)}$ , of the soft anomalous dimension matrix for  $q\bar{q} \rightarrow Q\bar{Q}$ , as a function of  $\Delta\eta$  for  $Y = 1$  and  $m_Q = m_t$  with resonance mass  $M = 1.5$  TeV and  $M = 750$  GeV for (a) and (b), respectively. The solid lines identify the quasi-singlet exponent,  $E_{11}^{(f)}$ , the dashed lines, quasi-octet,  $E_{22}^{(f)}$ , obtained from Eq. (16).

shown in Fig. 5. Following the discussion below Eq. (53), a smaller value of the exponent  $E_{22}^{(f)}$  enhances the factor  $[\ln(\frac{Q_0}{\Lambda}) / \ln(\frac{p_T}{\Lambda})]^{E_{22}^{(f)}}$  in the partonic cross section (53) relative to a larger value. We note that off-diagonal contributions are small.

The resulting gap fractions for two different spin-1 resonances,  $Z'$  and  $G$ , of mass 2 TeV, 1.5 TeV, 750 GeV, and 550 GeV are illustrated as functions of  $Q_0$  in Fig. 6 as the solid and the dashed curves for a top pair, and as the dot-dashed and the dotted curves (blue) for a bottom pair at fixed  $Y = 1.5$  and  $\Delta\eta = 2$ . The ratios of gap fractions,  $f_{gap}^G/f_{gap}^{Z'}$ , are shown in Fig. 7 at fixed  $Q_0 = 5$  GeV in terms of  $Y$  and  $\Delta\eta$  for  $M = 1.5$  TeV and 750 GeV. We observe that for the ratios the dependence on  $\Delta\eta$  is negligible at fixed  $Y$ . Also, Fig. 7 shows that these ratios get larger at fixed  $Q_0$  as the gap range increases.

In Figs. 8 and 9, the gap fractions and their ratios are presented as functions of  $Q_0$  and  $Y$  for  $M = 1.5$  TeV and 750 GeV, respectively. The gap fraction for an octet resonance increases rapidly for small values of  $Q_0$  in comparison to a singlet resonance for any gap size. Many fewer events are accumulated at low  $Q_0$  through a color-singlet resonance than for a color-octet resonance. For instance, at  $Q_0 = 3$  GeV and  $V'(1.5 \text{ TeV}, sp = 1)$  in Fig. 6(b), we obtain gap fractions of 12% and 54% for color-singlet and -octet resonances, respectively. The figures also show that the ratios are larger for larger  $M$  and  $Y$ .

We can interpret these results as follows. As we saw in Eq. (41) of Sec. 3, the eigenvectors,  $e_1$  and  $e_2$ , of the soft anomalous dimension matrix for  $q\bar{q} \rightarrow Q\bar{Q}$  are very close to a color singlet and a color octet for the kinematics and the gap geometry we study in this section. For this reason, we have called them “quasi-singlet” and “quasi-octet” eigenvectors, respectively. Consequently, this leads the hard functions in Eqs. (49) and (50) to retain approximately their color basis dependence even after transforming the functions to the diagonal basis.

Following the above property of the hard functions and the eigenvalues, shown in Fig. 4(a) for  $q\bar{q} \rightarrow Q\bar{Q}$ , the quasi-octet component of the hard function for a color octet resonance is the leading component, with a corresponding small exponent,  $E_{22}^{(f)}$ . We thus find that the quasi-octet cross section  $(H_G^{(f,LO)})_{22} S_{22}^{(f,0)} \left[ \frac{\ln(\frac{Q_0}{\Lambda})}{\ln(\frac{p_T}{\Lambda})} \right]^{E_{22}^{(f)}}$  is dominant in the partonic gap cross section (53) for an octet resonance  $G$ . The quasi-octet cross section is enhanced due to its large overlap with the color-octet basis which gives a small exponent  $E_{22} < 1$ . It is clear that this term produces the “convex” shapes of the dashed gap fraction curves ( $f_{gap}$ ) of the log plot on the  $x$ -axis, as shown in Fig. 6, and the upper surfaces in Figs. 8 and 9 for top

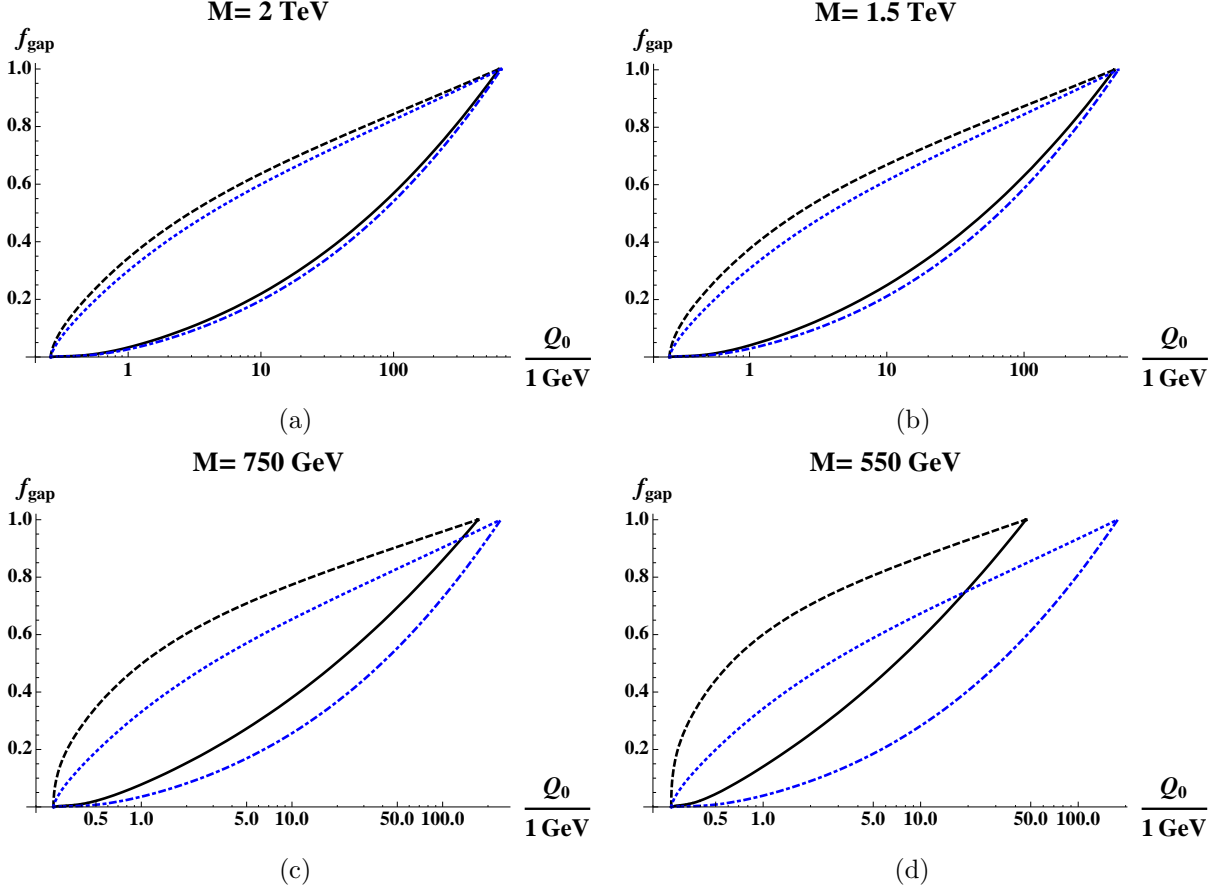


Figure 6: The fractions for gaps identified by the energy threshold  $Q_0$  at  $\Delta\eta = 2$  and  $Y = 1.5$  for resonance masses  $M = 2, 1.5, 0.75$ , and  $0.55 \text{ TeV}$ . In the above figures, the solid curves describe the gap fraction through a  $Z'$  resonance (color-singlet), and the dashed curves throughout a  $G$  resonance (color-octet) into a *top* quark pair. The dot-dashed curves (blue) describe the gap fraction through a  $Z'$  resonance (color-singlet), and the dotted curves (blue) throughout a  $G$  resonance (color-octet) into a *bottom* pair.



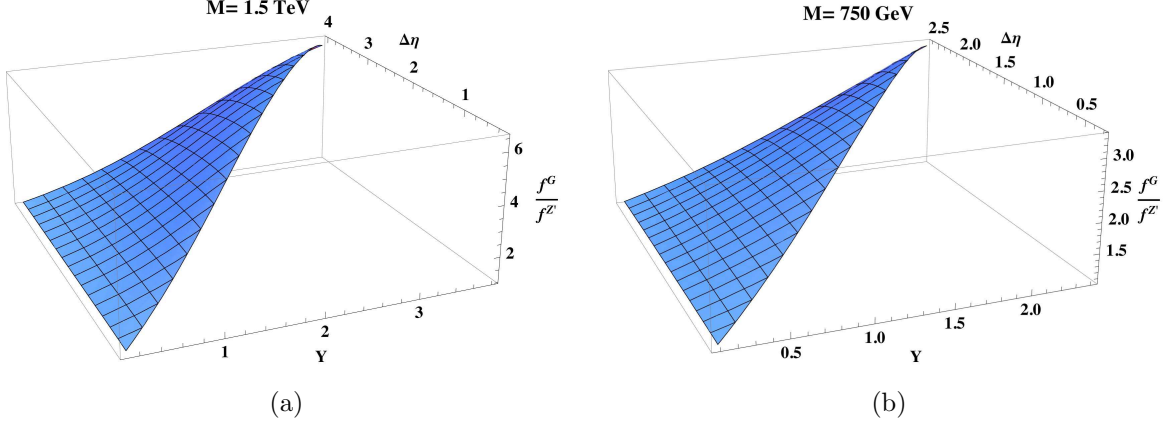


Figure 7: The ratios of two different gap fractions,  $f_{gap}^G/f_{gap}^{Z'}$ , as functions of  $Y$  and  $\Delta\eta$  at fixed  $Q_0 = 5$  GeV are shown (a) for  $M = 1.5$  TeV and (b)  $M = 750$  GeV, respectively.

pair production. These curves rise rapidly at low  $Q_0$ .

The singlet resonance process, on the other hand, has a larger overlap with the quasi-singlet component of the hard function. The eigenvalue of the quasi-singlet is larger than one, and  $E_{11}^{(f)} = (4/\beta_0)\text{Re } \lambda_1^{(f,1)} > 1$ . Thus, the quasi-singlet cross section,  $(H_{Z'}^{(f,LO)})_{11} S_{11}^{(f,0)} \left[ \frac{\ln(\frac{Q_0}{\Lambda})}{\ln(\frac{p_T}{\Lambda})} \right]^{E_{11}^{(f)}}$ , is suppressed at low  $Q_0$ , explaining the “concave” shapes of the solid lines in Fig. 6 and the lower surfaces in Figs. 8 and 9 for top pair production. These increase slowly at low  $Q_0$ . The differential partonic cross sections with respect to  $Q_c$  are presented in Fig. 10 for octet and singlet resonance processes for values  $M = 1.5$  TeV,  $\Delta\eta = 2.5$ , and  $Y = 1.5$ . The behavior of the exponents corresponds to the dominance of the octet resonance process at low  $Q_c$  in Fig. 10.

The gap fraction depends on the quark mass,  $m_Q$ , through the variable  $\rho$  in Eq. (11). The dependence can be seen in Fig. 6 by comparing the black curves (solid and dashed) for a top pair with the blue curves (dotted and dot-dashed) for a bottom pair. For the  $b$  quark, the gap fractions are slightly smaller at fixed gap threshold energy than for a top quark pair for the relatively heavy resonances in Fig. 6. This difference is, however, larger for smaller resonance mass, as also shown in Fig. 6. We note that the quark mass dependence on the gap fraction for bottom quark pair production is negligible even for a resonance of relatively low mass, but not for a top pair. For instance, we obtain  $\rho = 1.0003$  for bottom pair production via a resonance of  $M = 550$  GeV with  $\Delta\eta = 2$ , while  $\rho = 3.8200$  for a top pair. This results in the very different shapes of the black curves compared to the blue curves in Fig. 6(d).

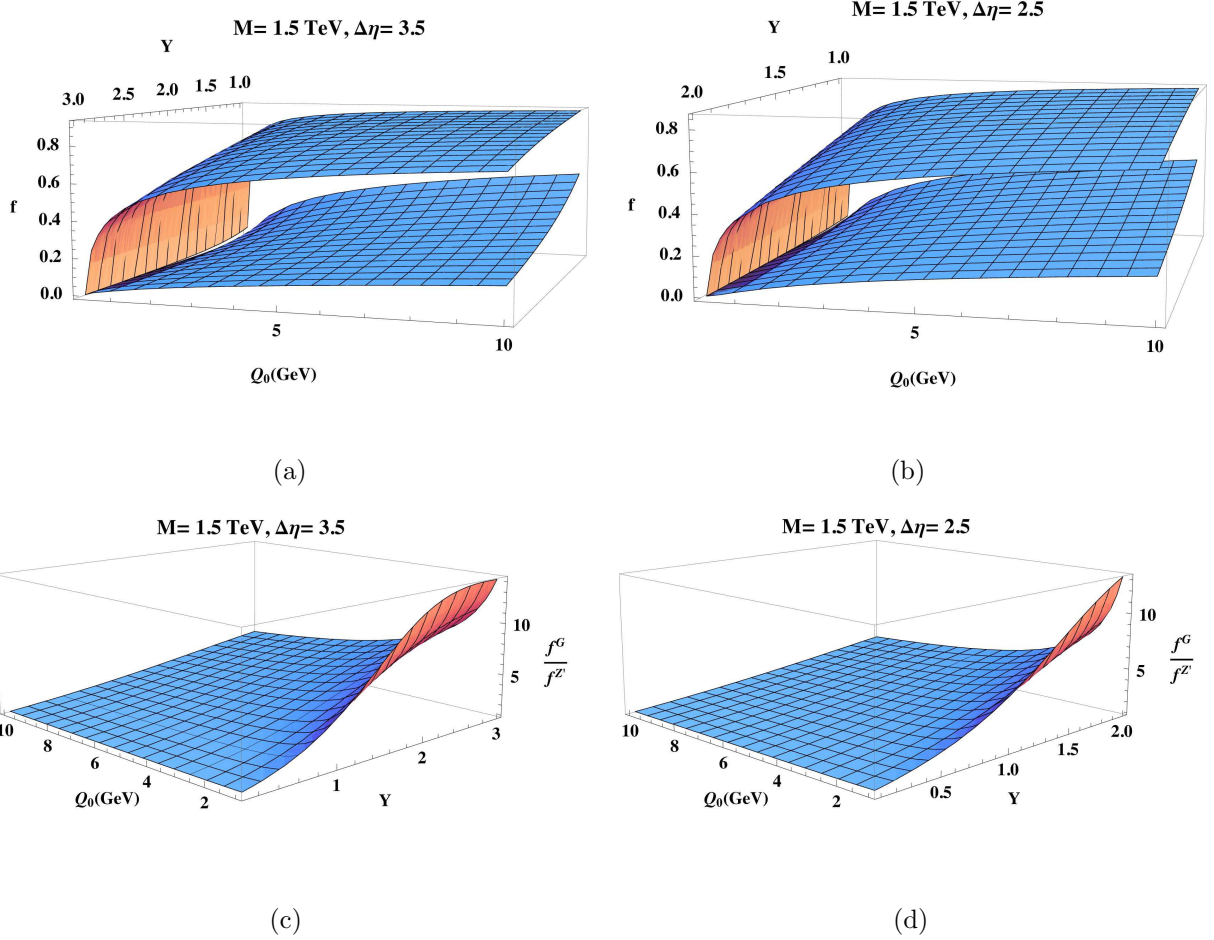
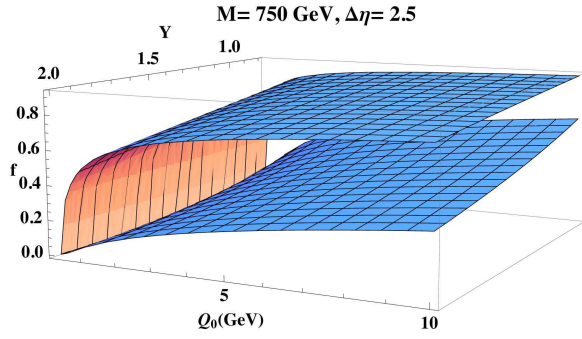
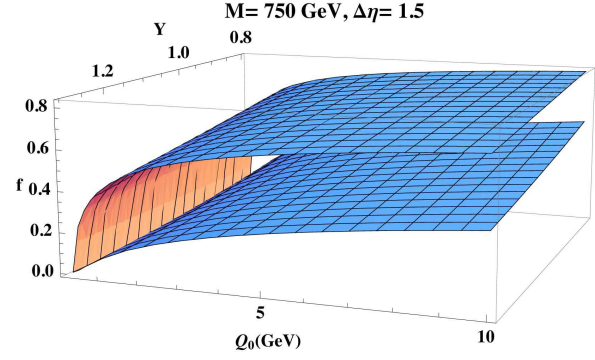


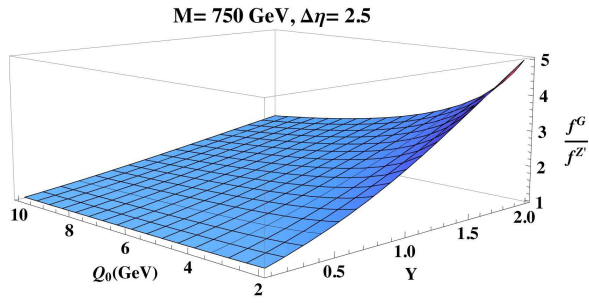
Figure 8: Gap fractions as functions of energy threshold  $Q_0$  and gap range  $Y$  from a resonance of  $M = 1.5 \text{ TeV}$ , (a) for  $\Delta\eta = 3.5$  and (b) for  $\Delta\eta = 2.5$ . The lower surfaces in (a) and (b) describe the gap fractions through a  $Z'$  resonance (color-singlet), the upper surfaces throughout a  $G$  resonance (color-octet) decaying into a top quark pair. The ratios of the gap fraction for an octet resonance to the gap fraction for a singlet resonance are illustrated in (c) and (d) as functions of  $Q_0$  and  $Y$ .



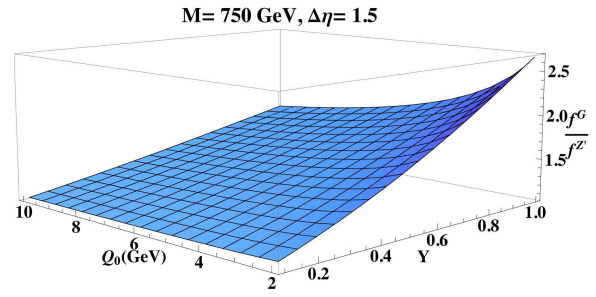
(a)



(b)



(c)



(d)

Figure 9: Same as Fig. 8, for  $M = 750 \text{ GeV}$ , in the allowed region in gap size  $Y$ .

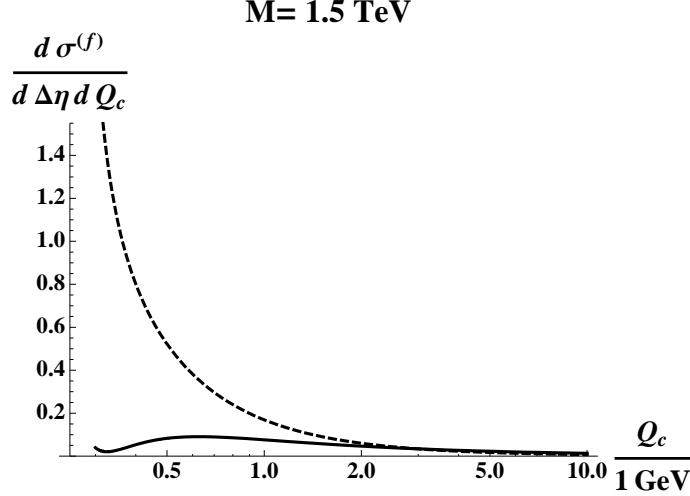


Figure 10: The cross section from the octet resonance (dashed line) and the singlet resonance (solid line) for  $M = 1.5$  TeV,  $\Delta\eta = 2.5$ , and  $Y = 1.5$ . Both distributions are normalized to the same area for the range of  $\Lambda < Q_c < p_T$ .

The results in this section show that the measurement of gap fractions can be an effective tool to identify the color content of a spin-1  $s$ -channel resonance. In the next section, we study gap fractions for spin-0 or 2 resonance processes, which contain more partonic channels.

## 6 Gap Fractions for Spin-0 or 2 Resonances

As we discussed briefly in Sec. 4, in several models of new physics, there are  $s$ -channel spin-0 and spin-2 resonances, decaying into a heavy quark pair, which can be produced, through gluon-induced processes in addition to quark-antiquark reactions. We readily recognize that spin-0 or 2 resonance processes might lead to a different pattern of soft gluon radiation between the Tevatron and the LHC, because of the presence of both quark and gluon-induced partonic processes. As we shall see, PDFs no longer cancel in the leading order gap fraction. This is distinguished from the analysis in Sec. 5 for spin-1 resonances, involving only one partonic channel. The results in Sec. 5 are energy-independent, at leading order, applying to both the Tevatron and the LHC.

Let's assume that there are two partonic processes that produce a heavy resonance, decaying into a heavy quark pair,  $f_1 : q\bar{q} \rightarrow V' \rightarrow Q\bar{Q}$  and  $f_2 : gg \rightarrow V' \rightarrow Q\bar{Q}$ . In addition, we assume for simplicity that the coupling of light quarks is universal. Recall that the process

$f_2$  cannot occur for a spin-1 resonance in general. Therefore, we consider the octet resonance as spin-0 or 2. In this case, we obtain the gap fraction, following Eq. (21),

$$\begin{aligned} f_{gap}^{(LO)} &= \frac{\int dx_1 dx_2 \left( \sum_{f_1 f_2} \frac{d\hat{\sigma}^{(f_1)}(Q_0)}{d\Delta\eta dM^2 d\eta_{V'}} \phi_{f_1/A}(x_1) \phi_{f_2/B}(x_2) + \frac{d\hat{\sigma}^{(f_2)}(Q_0)}{d\Delta\eta dM^2 d\eta_{V'}} \phi_{g/A}(x_1) \phi_{g/B}(x_2) \right)}{\int dx_1 dx_2 \left( \sum_{f_1 f_2} \frac{d\hat{\sigma}^{(f_1, LO)}}{d\Delta\eta dM^2 d\eta_{V'}} \phi_{f_1/A}(x_1) \phi_{f_2/B}(x_2) + \frac{d\hat{\sigma}^{(f_2, LO)}}{d\Delta\eta dM^2 d\eta_{V'}} \phi_{g/A}(x_1) \phi_{g/B}(x_2) \right)} \\ &= p^{q\bar{q} \rightarrow Q\bar{Q}} f_{gap}^{q\bar{q} \rightarrow Q\bar{Q}} + p^{gg \rightarrow Q\bar{Q}} f_{gap}^{gg \rightarrow Q\bar{Q}}, \end{aligned} \quad (55)$$

where the  $p^{f_i}$  are defined by

$$\begin{aligned} p^{q\bar{q} \rightarrow Q\bar{Q}} &\equiv \frac{\frac{d\hat{\sigma}^{(f_1, LO)}}{d\Delta\eta} \left( \sum_{f_1 f_2} \phi_{f_1/A}(x_1) \phi_{f_2/B}(x_2) \right)}{\frac{d\hat{\sigma}^{(f_1, LO)}}{d\Delta\eta} \left( \sum_{f_1 f_2} \phi_{f_1/A}(x_1) \phi_{f_2/B}(x_2) \right) + \frac{d\hat{\sigma}^{(f_2, LO)}}{d\Delta\eta} \phi_{f_g/A}(x_1) \phi_{f_g/B}(x_2)}, \\ p^{gg \rightarrow Q\bar{Q}} &\equiv \frac{\frac{d\hat{\sigma}^{(f_2, LO)}}{d\Delta\eta} \phi_{f_g/A}(x_1) \phi_{f_g/B}(x_2)}{\frac{d\hat{\sigma}^{(f_1, LO)}}{d\Delta\eta} \left( \sum_{f_1 f_2} \phi_{f_1/A}(x_1) \phi_{f_2/B}(x_2) \right) + \frac{d\hat{\sigma}^{(f_2, LO)}}{d\Delta\eta} \phi_{f_g/A}(x_1) \phi_{f_g/B}(x_2)}, \end{aligned} \quad (56)$$

and the gap fractions,  $f_{gap}^{q\bar{q} \rightarrow Q\bar{Q}}$  and  $f_{gap}^{gg \rightarrow Q\bar{Q}}$ , are given by

$$f_{gap}^{q\bar{q} \rightarrow Q\bar{Q}}(Q_0) = \frac{\frac{d\hat{\sigma}^{(f_1)}(Q_0)}{d\Delta\eta}}{\frac{d\hat{\sigma}^{(f_1, LO)}}{d\Delta\eta}}, \quad f_{gap}^{gg \rightarrow Q\bar{Q}}(Q_0) = \frac{\frac{d\hat{\sigma}^{(f_2)}(Q_0)}{d\Delta\eta}}{\frac{d\hat{\sigma}^{(f_2, LO)}}{d\Delta\eta}}, \quad (57)$$

which can be calculated perturbatively, following Eqs. (18) and (19). We can interpret the  $p^{f_i}$  as the probability for the process  $f_i$  among the channels,  $p^{q\bar{q} \rightarrow Q\bar{Q}} + p^{gg \rightarrow Q\bar{Q}} = 1$ .

We can study the above gap fraction for representative choices of  $p^{q\bar{q} \rightarrow Q\bar{Q}}$  and  $p^{gg \rightarrow Q\bar{Q}}$ . For the first example, we compare the gap fraction for an octet resonance with the gap fraction for a singlet resonance through a pure gluon-induced process,  $p^{gg \rightarrow Q\bar{Q}} = 1$  and  $p^{q\bar{q} \rightarrow Q\bar{Q}} = 0$ . A pseudo-scalar or a boson-phobic scalar resonance is a good example for the above resonance process, where gluon-induced processes are dominant and the branching ratio to a top pair can be taken to be unity [26]. In general, SUSY models with this feature can be constructed for singlet resonances [75], and split SUSY scenarios can explain octet resonances from bound states of meta-stable gluinos [76].

The gap fractions for the pure gluon-induced resonances are determined by the soft anomalous dimension matrix in Eq. (44), its eigenvalues and eigenvectors for the process  $gg \rightarrow Q\bar{Q}$ . The resulting gap fractions for octet and singlet resonances are illustrated in Fig. 11(a) for  $M = 1.5$  TeV,  $\Delta\eta = 2.5$ , and  $Y = 1$ .

To study the effect of an admixture of quark- and gluon-induced processes, the gap fraction for an octet resonance with  $p^{gg \rightarrow Q\bar{Q}} = 0.8$  and  $p^{q\bar{q} \rightarrow Q\bar{Q}} = 0.2$  is represented in

Fig. 11(b) as a dashed curve in comparison to the gap fraction for the pure gluon-induced singlet resonance, shown as a solid curve in the same figure. This quark/gluon admixture for an octet resonance can occur for the reggeon resonances of Ref. [74].

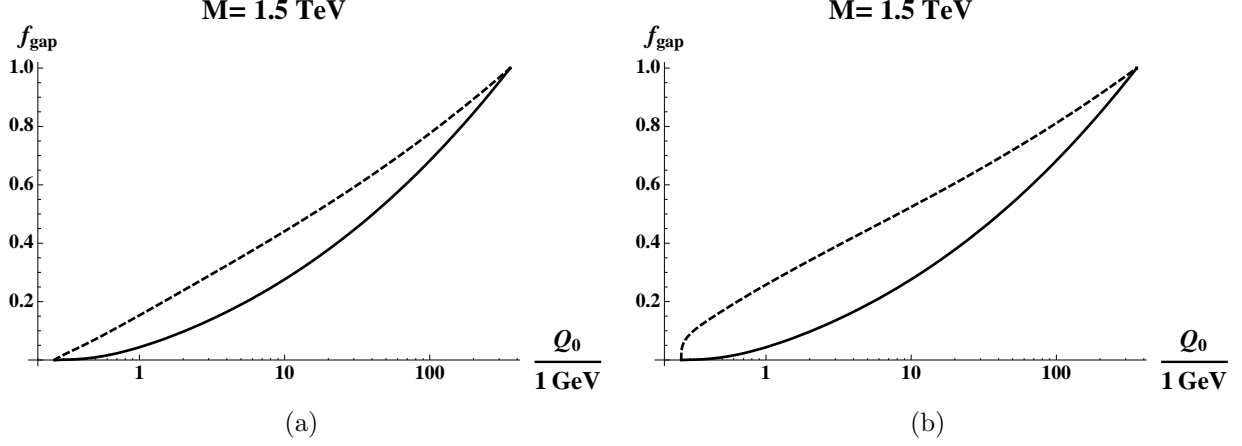


Figure 11: Gap fraction as a function of gap energy threshold  $Q_0$  at  $\Delta\eta = 2.5$  with  $M = 1.5$  TeV and  $Y = 1$ . In (a) and (b), the solid lines describe the gap fraction through a  $Z'$  resonance (color-singlet) for  $p^{gg \rightarrow Q\bar{Q}} = 1$ . The dashed line describes the gap fraction through a  $G$  resonance (color-octet) in (a) for  $p^{gg \rightarrow Q\bar{Q}} = 1$  and in (b) for  $p^{gg \rightarrow Q\bar{Q}} = 0.8$  and  $p^{q\bar{q} \rightarrow Q\bar{Q}} = 0.2$ .

As observed in the previous section, we again see in Fig. 11(a) that there is “less” radiation into the gap region for the color-octet resonance process. At the same time, we notice that for the same resonances there is “more” radiation for gluon-induced processes than for quark-induced processes. This can be seen by comparing solid and dashed curves in Fig. 6 with the curves in Fig. 11(a).

Scattered gluons tend to emit more radiation, compared to scattered quarks. We note that the shape of the gap fraction for gluon-induced octet resonances in Fig. 11(a) is “linear”, while the shape for quark-induced octet resonances in Fig. 6 is “convex”. Following the arguments in the previous section, the values of the exponents for gluon-induced processes in Fig. 12 can account for the difference. The eigenvalues for the process  $gg \rightarrow Q\bar{Q}$  in Fig. 13 ensure that all exponents  $E_{\alpha\beta}^{(gg \rightarrow Q\bar{Q})}$  are larger than one for  $Y$  of order unity, as shown in Fig. 12. We note that two quasi-octet eigenvectors,  $e_2$  and  $e_3$ , of  $\Gamma_S^{(gg \rightarrow Q\bar{Q})}$  in Eq. (44), which we recall are determined numerically, turn out to approach  $e_2$  and  $e_3$  in Eq. (47), obtained in large  $N_c$  limit. As a result, both the quasi-octet components,  $(H'_G)_{22}$  and  $(H'_G)_{33}$ , of the octet hard function, written in the basis that diagonalizes  $\Gamma_S^{(1)(gg \rightarrow Q\bar{Q})}$ , are important. Their exponents,  $E_{22}^{(gg \rightarrow Q\bar{Q})}$  and  $E_{33}^{(gg \rightarrow Q\bar{Q})}$ , are shown as the dashed and the dot-dashed lines

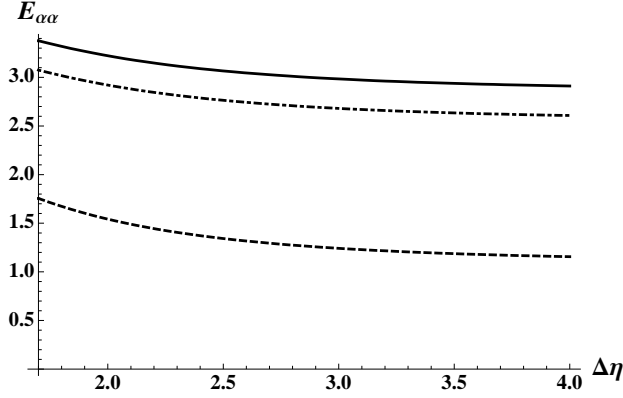


Figure 12: Plot of the exponents,  $E_{\alpha\alpha}^{(f)}$ , of the soft anomalous dimension matrix for  $gg \rightarrow Q\bar{Q}$  as a function of  $\Delta\eta$  for  $Y = 1.5$  and  $m_Q = m_t$  with resonance mass  $M = 1.5$  TeV. The solid line identifies the quasi-singlet exponent, the dashed and the dot-dashed lines the two quasi-octets.

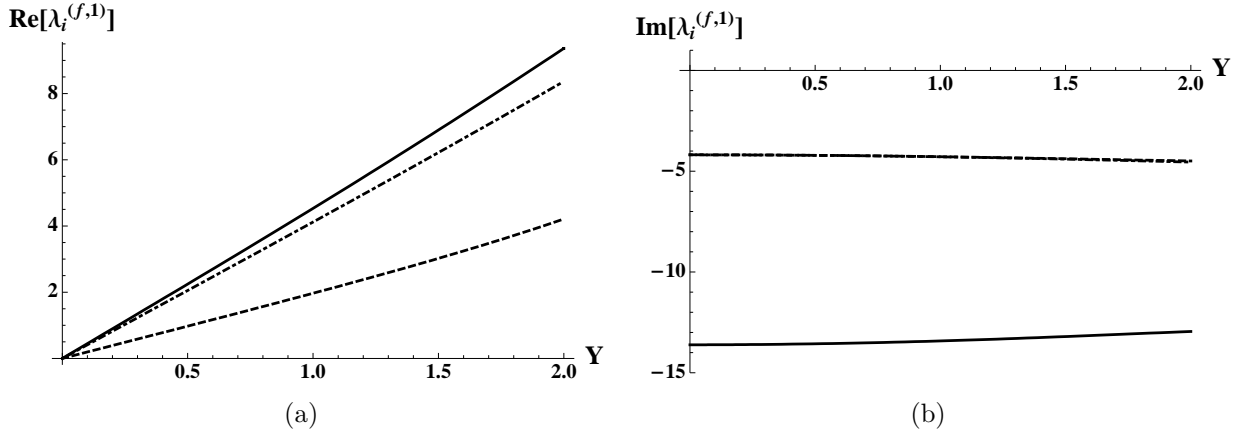


Figure 13: Plot of the real (a) and imaginary (b) parts of the eigenvalues of the soft anomalous dimension matrix for  $gg \rightarrow Q\bar{Q}$  of  $M = 1.5$  TeV,  $\Delta\eta = 2.5$  and  $m_Q = m_t$ . The solid line identifies the quasi-singlet eigenvalue, the dashed and the dot-dashed lines the two quasi-octets.

in Fig. 12. An interesting feature is that one of the quasi-octet exponents is close to the exponent for a quasi-singlet. A semi-numerical expression for the cross section (18) for gluon-induced octet resonances is given for  $M = 1.5$  TeV,  $Y = 1$ , and  $\Delta\eta = 1.5$  by

$$\begin{aligned} \frac{d\hat{\sigma}_G^{(gg \rightarrow Q\bar{Q})}}{d\Delta\eta} &= \sum_{\beta,\gamma} (H_G'^{(f_2, LO)})_{\beta\gamma} S_{\gamma\beta}^{(f_2, 0)} \left[ \frac{\ln(\frac{Q_0}{\Lambda})}{\ln(\frac{p_T}{\Lambda})} \right]^{E_{\gamma\beta}^{(f)}} \\ &\simeq h'_G \left( (0.23) \left[ \frac{\ln(\frac{Q_0}{\Lambda})}{\ln(\frac{p_T}{\Lambda})} \right]^{2.27} + (6.19) \left[ \frac{\ln(\frac{Q_0}{\Lambda})}{\ln(\frac{p_T}{\Lambda})} \right]^{2.08} + (6.33) \left[ \frac{\ln(\frac{Q_0}{\Lambda})}{\ln(\frac{p_T}{\Lambda})} \right]^{1.17} \right), \end{aligned} \quad (58)$$

where the first coefficient, 0.23, of second line in Eq. (58) is  $(H_G'^{(f_2, LO)})_{11} S_{11}^{(f_2, 0)}$ , and the other two, 6.19 and 6.33, are  $(H_G'^{(f_2, LO)})_{22} S_{22}^{(f_2, 0)}$  and  $(H_G'^{(f_2, LO)})_{33} S_{33}^{(f_2, 0)}$ , respectively. Here  $h'_G$  has been defined in Eq. (51). In Eq. (58), we omit off-diagonal contributions such as  $(H_G'^{(f_2, LO)})_{23} S_{32}^{(f_2, 0)}$ , because they contribute less than 2% of the total. We observe that each  $Q_0$ -dependent factor,  $[\ln(\frac{Q_0}{\Lambda}) / \ln(\frac{p_T}{\Lambda})]^{E_{\alpha\beta}^{(gg \rightarrow Q\bar{Q})}}$ , is thus suppressed, relative to linear behavior in a log plot at low  $Q_0$ , for all quasi-octet exponents in the partonic cross section (58). This explains why the dashed curve in Fig. 11(a) increases slowly at low  $Q_0$  compared to the dashed curves in Fig. 6(b).

In Fig. 11, the dashed curve for a pure gluon-induced process in (a) shows a smaller gap fraction than the dashed curve for a mixed quark-gluon process in (b) for given  $Q_0$ . As we discussed in the previous section, the gap fraction for  $q\bar{q} \rightarrow Q\bar{Q}$  rises rapidly at low  $Q_0$ . The term,  $f_{gap}^{q\bar{q} \rightarrow Q\bar{Q}}$ , even with the small assumed probability  $p^{q\bar{q} \rightarrow Q\bar{Q}} = 0.2$  thus explains the difference of the dashed curves in Fig. 11. We note that the shape of the solid curves for  $gg \rightarrow Z' \rightarrow Q\bar{Q}$  in Fig. 11 corresponds to the largest amount of radiation among the resonance processes we have studied in this paper. This is due to the large quasi-singlet exponent  $E_{11}^{(gg \rightarrow Q\bar{Q})}$ , compared to other exponents.

The above results, depending on partonic channels and the gauge content of resonances, can be understood intuitively in terms of color dipole configurations. In Fig. 14, the color dipole structures and the preferred directions of radiation are represented as solid curves and arrows, respectively. Each figure describes the surplus of radiation inside a dipole [58–60]. For examples, the dipole configurations in Figs. 14(a) and 14(c) allow more radiation into the  $Q\bar{Q}$  region, which overlaps the gap region, while the configuration for  $q\bar{q} \rightarrow G \rightarrow Q\bar{Q}$  in Fig. 14(d) describes enhanced radiation in the  $qQ$  and the  $\bar{q}\bar{Q}$  regions that are outside the gap region. In Fig. 14(b), the color-(anti)symmetric couplings control the dipole configuration, which results



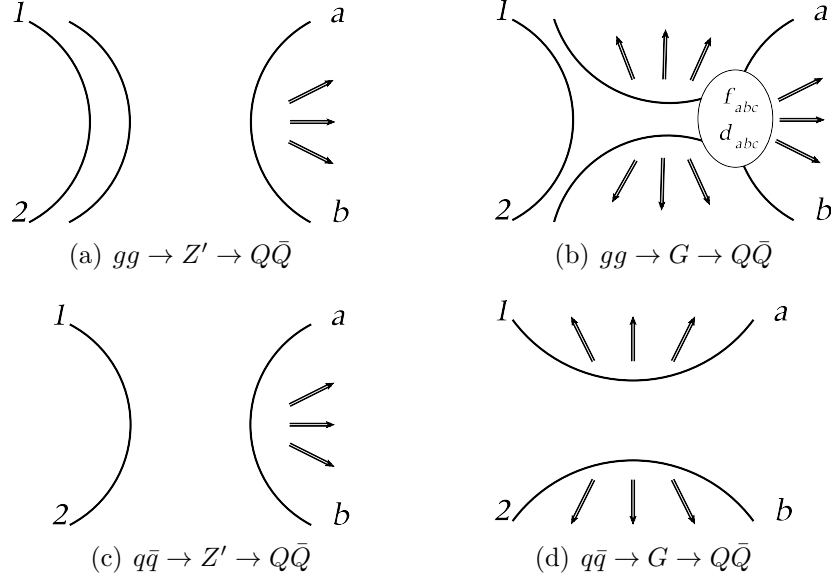


Figure 14: Color dipole configurations for resonance processes,  $f_1(p_1) + f_2(p_2) \rightarrow V' \rightarrow Q(p_a) + \bar{Q}(p_b)$ . Arrows in each figure represent the enhanced direction of radiation.

in radiation into both the  $qQ$  and the  $Q\bar{Q}$  regions. We have also predicted the least(most) amount of radiation into the gap region for  $q\bar{q} \rightarrow G \rightarrow Q\bar{Q}$  ( $gg \rightarrow Z' \rightarrow Q\bar{Q}$ ). These color dipole configurations help explain our results for the patterns of radiation, associated with the SU(3) color representation of resonances and the partonic channels involved.

At the end of Sec. 3, we argued that for a narrow resonance, generally a gauge singlet, there is an additional contribution when the radiation energy scale is larger than  $\sqrt{\Gamma M}$ . In this limit, we expect that the color dipole configuration is further dominant since the process becomes a pure color singlet decay. This contribution is expected to be absent for an octet resonance since the width is in general large. We point out that this may result in more radiation for a very narrow singlet resonance process compared to our results in Secs. 5 and 6, leading an even more distinguishable difference from an octet resonance process. The details of this case are left for future work.

## 7 Conclusion

In this paper, we have shown that it may be possible to determine the color SU(3) representation of resonances from new physics signals by analyzing the distribution of soft radiation

into a rapidity gap. The results we have found are based on perturbative calculations of factorized partonic cross sections, and apply for ordered scales,  $\Lambda_{QCD} < Q_c < \sqrt{\Gamma M} \sim p_T$  with energy flow,  $Q_c$ , resonance mass,  $M$ , and decay width,  $\Gamma$ . These conditions correspond to a broad width resonance process. The gap fractions for octet and singlet resonances, which we defined in Sec. 2.3, show different radiation patterns of energy flow. To obtain an analytical form of soft gluon emission in heavy quark pair production, the massive soft anomalous dimension matrix for rapidity gap events was introduced. The results, in general, describe more radiation for singlet than for octet resonances, which can be explained in terms of color dipole configurations. Especially, for spin-1 resonance production, involving only one partonic sub-process, we obtained a relatively large difference in radiation into the gap region between color singlet and octet resonances. The results at leading order do not require a convolution with PDFs, and are the same at the Tevatron and the LHC in this case. At the end of Sec. 6, we discussed the consequences of a narrow width resonance, expecting more radiation for a singlet resonance process compared to our results based on a broad resonance assumption.

In principle, following Ref. [11], given any fixed set of final-state partons, we may calculate the distribution of energy flow into any fixed region of rapidity and azimuthal angle rather than the simple rapidity gap we defined in this paper. This may allow not only to illuminate more distinguishable features of color flow, depending on the gauge content of resonances, but also to shed valuable light on the dynamics of QCD radiation itself.

## Acknowledgements

I would like to express my gratitude to George Sterman, for many conversations and comments on the manuscript, and for all his help. I am indebted to Gilad Perez and Zuowei Liu for their valuable advice, and to Leo Almeida, Rikkert Frederix and Alex Mitov for discussions. This work was supported in part by the National Science Foundation, PHY-0354776, PHY-0354822 and PHY-0653342.

# Appendix

In general, we represent the four momentum of a particle of mass  $m_Q$  as

$$p^\mu = (m_T \cosh \eta, p_x, p_y, m_T \sinh \eta) , \quad (\text{A.1})$$

where  $\eta$  is rapidity and where  $m_T$  is a transverse mass defined by

$$m_T^2 = m_Q^2 + p_x^2 + p_y^2 = m_Q^2 + p_T^2 . \quad (\text{A.2})$$

In the  $\eta$ - $\phi$  coordinate system of rapidity and azimuthal angle, four momentum  $p^\mu$  can be written in terms of quark mass  $m_Q$  and  $\phi$  as

$$p^\mu = \left( \sqrt{p_T^2 + m_Q^2} \cosh \eta, p_T \sin \phi, p_T \cos \phi, \sqrt{p_T^2 + m_Q^2} \sinh \eta \right) . \quad (\text{A.3})$$

To describe the process in Eq. (1) with the gap geometry, shown in Fig. 1 at lowest order, we need five external partons of momenta

$$\begin{aligned} p_1^\mu &= \frac{\sqrt{\hat{s}}}{2} (1, 0, 0, 1) , \\ p_2^\mu &= \frac{\sqrt{\hat{s}}}{2} (1, 0, 0, -1) , \\ p_a^\mu &= \left( \sqrt{p_T^2 + m_Q^2} \cosh \left( \frac{\Delta\eta}{2} \right), 0, p_T, \sqrt{p_T^2 + m_Q^2} \sinh \left( \frac{\Delta\eta}{2} \right) \right) , \\ p_a^\mu &= \left( \sqrt{p_T^2 + m_Q^2} \cosh \left( \frac{\Delta\eta}{2} \right), 0, -p_T, -\sqrt{p_T^2 + m_Q^2} \sinh \left( \frac{\Delta\eta}{2} \right) \right) , \\ k^\mu &= k_T (\cosh y, \sin \phi, \cos \phi, \sinh y) , \end{aligned} \quad (\text{A.4})$$

where we are working in the partonic center of mass frame, and where we fix azimuthal angles for a quark pair at  $\phi_a = 0$  and  $\phi_b = \pi$ . Here  $y$  is rapidity of soft gluon  $k$ .

# References

- [1] J. C. Collins, D. E. Soper and G. Sterman, Adv. Ser. Direct. High Energy Phys. **5**, 1 (1988) [arXiv:hep-ph/0409313]; G. Sterman, arXiv:hep-ph/0412013.
- [2] H. Contopanagos, E. Laenen and G. Sterman, Nucl. Phys. B **484**, 303 (1997) [arXiv:hep-ph/9604313].

- [3] A. Sen, Phys. Rev. D **24**, 3281 (1981).
- [4] J. Botts and G. Sterman, Nucl. Phys. B **325**, 62 (1989).
- [5] M. Derrick *et al.* [ZEUS Collaboration], Phys. Lett. B **369**, 55 (1996) [arXiv:hep-ex/9510012].
- [6] S. Chekanov *et al.* [ZEUS Collaboration], arXiv:hep-ex/0612008.
- [7] C. Adloff *et al.* [H1 Collaboration], Eur. Phys. J. C **24**, 517 (2002) [arXiv:hep-ex/0203011].
- [8] S. Abachi *et al.* [D0 Collaboration], Phys. Rev. Lett. **76**, 734 (1996) [arXiv:hep-ex/9509013]; F. Abe *et al.* [CDF Collaboration], Phys. Rev. Lett. **80**, 1156 (1998); F. Abe *et al.* [CDF Collaboration], Phys. Rev. Lett. **74**, 855 (1995).
- [9] J. D. Bjorken, Phys. Rev. D **47**, 101 (1993).
- [10] G. Oderda and G. Sterman, Phys. Rev. Lett. **81**, 3591 (1998) [arXiv:hep-ph/9806530].
- [11] C. F. Berger, T. Kucs and G. Sterman, Phys. Rev. D **65**, 094031 (2002) [arXiv:hep-ph/0110004].
- [12] R. B. Appleby and M. H. Seymour, JHEP **0309**, 056 (2003) [arXiv:hep-ph/0308086].
- [13] A. Kyrieleis and M. H. Seymour, JHEP **0601**, 085 (2006) [arXiv:hep-ph/0510089].
- [14] M. Sjodahl, JHEP **0812**, 083 (2008) [arXiv:0807.0555 [hep-ph]].
- [15] M. Sjodahl, arXiv:0906.1121 [hep-ph].
- [16] M. Dasgupta and G. P. Salam, Phys. Lett. B **512**, 323 (2001) [arXiv:hep-ph/0104277].
- [17] M. Dasgupta and G. P. Salam, JHEP **0203**, 017 (2002) [arXiv:hep-ph/0203009].
- [18] J. R. Forshaw, A. Kyrieleis and M. H. Seymour, JHEP **0608**, 059 (2006) [arXiv:hep-ph/0604094].
- [19] J. R. Forshaw, A. Kyrieleis and M. H. Seymour, JHEP **0809**, 128 (2008) [arXiv:0808.1269 [hep-ph]].
- [20] J. Keates and M. H. Seymour, JHEP **0904**, 040 (2009) [arXiv:0902.0477 [hep-ph]].

- [21] R. B. Appleby and M. H. Seymour, JHEP **0212**, 063 (2002) [arXiv:hep-ph/0211426].
- [22] J. Forshaw, J. Keates and S. Marzani, JHEP **0907**, 023 (2009) [arXiv:0905.1350 [hep-ph]].
- [23] J. R. Forshaw and M. Sjodahl, JHEP **0709**, 119 (2007) [arXiv:0705.1504 [hep-ph]].
- [24] A. Kulesza and L. Motyka, Phys. Rev. Lett. **102**, 111802 (2009) [arXiv:0807.2405 [hep-ph]].
- [25] A. Kulesza and L. Motyka, arXiv:0905.4749 [hep-ph].
- [26] R. Frederix and F. Maltoni, JHEP **0901**, 047 (2009) [arXiv:0712.2355 [hep-ph]].
- [27] K. Agashe, A. Belyaev, T. Krupovnickas, G. Perez and J. Virzi, Phys. Rev. D **77**, 015003 (2008) [arXiv:hep-ph/0612015].
- [28] A. L. Fitzpatrick, J. Kaplan, L. Randall and L. T. Wang, JHEP **0709**, 013 (2007) [arXiv:hep-ph/0701150].
- [29] B. Lillie, L. Randall and L. T. Wang, JHEP **0709**, 074 (2007) [arXiv:hep-ph/0701166].
- [30] K. Agashe, H. Davoudiasl, G. Perez and A. Soni, Phys. Rev. D **76**, 036006 (2007) [arXiv:hep-ph/0701186].
- [31] K. Agashe *et al.*, Phys. Rev. D **76**, 115015 (2007) [arXiv:0709.0007 [hep-ph]].
- [32] U. Baur and L. H. Orr, Phys. Rev. D **77**, 114001 (2008) [arXiv:0803.1160 [hep-ph]].
- [33] K. Agashe, S. Gopalakrishna, T. Han, G. Y. Huang and A. Soni, arXiv:0810.1497 [hep-ph].
- [34] H. Davoudiasl, S. Gopalakrishna and A. Soni, arXiv:0908.1131 [hep-ph].
- [35] J. M. Butterworth, A. R. Davison, M. Rubin and G. P. Salam, Phys. Rev. Lett. **100**, 242001 (2008) [arXiv:0802.2470 [hep-ph]].
- [36] J. Thaler and L. T. Wang, JHEP **0807**, 092 (2008) [arXiv:0806.0023 [hep-ph]].
- [37] D. E. Kaplan, K. Rehermann, M. D. Schwartz and B. Tweedie, Phys. Rev. Lett. **101**, 142001 (2008) [arXiv:0806.0848 [hep-ph]].

- [38] L. G. Almeida, S. J. Lee, G. Perez, G. Sterman, I. Sung and J. Virzi, Phys. Rev. D **79**, 074017 (2009) [arXiv:0807.0234 [hep-ph]].
- [39] L. G. Almeida, S. J. Lee, G. Perez, I. Sung and J. Virzi, Phys. Rev. D **79**, 074012 (2009) [arXiv:0810.0934 [hep-ph]].
- [40] S. Godfrey and T. A. W. Martin, Phys. Rev. Lett. **101**, 151803 (2008) [arXiv:0807.1080 [hep-ph]].
- [41] P. Fileviez Perez, R. Gavin, T. McElmurry and F. Petriello, Phys. Rev. D **78**, 115017 (2008) [arXiv:0809.2106 [hep-ph]].
- [42] S. D. Ellis, C. K. Vermilion and J. R. Walsh, arXiv:0903.5081 [hep-ph].
- [43] L. T. Wang and I. Yavin, Int. J. Mod. Phys. A **23**, 4647 (2008) [arXiv:0802.2726 [hep-ph]].
- [44] N. Arkani-Hamed, S. Dimopoulos and G. R. Dvali, Phys. Lett. B **429**, 263 (1998) [arXiv:hep-ph/9803315].
- [45] L. Randall and R. Sundrum, Phys. Rev. Lett. **83**, 3370 (1999) [arXiv:hep-ph/9905221].
- [46] D. Dicus, A. Stange and S. Willenbrock, Phys. Lett. B **333**, 126 (1994) [arXiv:hep-ph/9404359].
- [47] W. Bernreuther, M. Flesch and P. Haberl, Phys. Rev. D **58**, 114031 (1998) [arXiv:hep-ph/9709284].
- [48] D. Choudhury, R. M. Godbole, R. K. Singh and K. Wagh, Phys. Lett. B **657**, 69 (2007) [arXiv:0705.1499 [hep-ph]].
- [49] N. Kidonakis and G. Sterman, Phys. Lett. B **387**, 867 (1996).
- [50] N. Kidonakis and G. Sterman, Nucl. Phys. B **505**, 321 (1997) [arXiv:hep-ph/9705234].
- [51] N. Kidonakis, G. Oderda and G. Sterman, Nucl. Phys. B **525**, 299 (1998) [arXiv:hep-ph/9801268].
- [52] N. Kidonakis, Phys. Rev. Lett. **102**, 232003 (2009) [arXiv:0903.2561 [hep-ph]].
- [53] A. Mitov, G. Sterman and I. Sung, Phys. Rev. D **79**, 094015 (2009) [arXiv:0903.3241 [hep-ph]].

- [54] T. Becher and M. Neubert, Phys. Rev. D **79**, 125004 (2009) [arXiv:0904.1021 [hep-ph]].
- [55] M. Beneke, P. Falgari and C. Schwinn, arXiv:0907.1443 [hep-ph].
- [56] M. Czakon, A. Mitov and G. Sterman, arXiv:0907.1790 [hep-ph].
- [57] A. Ferroglia, M. Neubert, B. D. Pecjak and L. L. Yang, arXiv:0907.4791 [hep-ph].
- [58] Y. L. Dokshitzer, V. A. Khoze and S. I. Troian, Adv. Ser. Direct. High Energy Phys. **5**, 241 (1988).
- [59] Y. L. Dokshitzer, V. A. Khoze, A. H. Mueller and S. I. Troian, *Gif-sur-Yvette, France: Ed. Frontieres (1991) 274 p. (Basics of)*.
- [60] R. K. Ellis, W. J. Stirling and B. R. Webber, Camb. Monogr. Part. Phys. Nucl. Phys. Cosmol. **8**, 1 (1996).
- [61] C. F. Berger, T. Kucs and G. Sterman, Phys. Rev. D **68**, 014012 (2003) [arXiv:hep-ph/0303051].
- [62] A. Banfi, G. P. Salam and G. Zanderighi, JHEP **0408**, 062 (2004) [arXiv:hep-ph/0407287].
- [63] G. Sterman, arXiv:hep-ph/0501270.
- [64] C. F. Berger, Mod. Phys. Lett. A **20**, 1187 (2005) [arXiv:hep-ph/0505037].
- [65] A. Djouadi, G. Moreau and R. K. Singh, Nucl. Phys. B **797**, 1 (2008) [arXiv:0706.4191 [hep-ph]].
- [66] R. M. Harris, C. T. Hill and S. J. Parke, arXiv:hep-ph/9911288.
- [67] N. Arkani-Hamed, A. G. Cohen, E. Katz and A. E. Nelson, JHEP **0207**, 034 (2002) [arXiv:hep-ph/0206021].
- [68] M. Schmaltz and D. Tucker-Smith, Ann. Rev. Nucl. Part. Sci. **55**, 229 (2005) [arXiv:hep-ph/0502182].
- [69] J. Boersma, Phys. Rev. D **74**, 115008 (2006) [arXiv:hep-ph/0608239].
- [70] J. Boersma and A. Whitbeck, Phys. Rev. D **77**, 055012 (2008) [arXiv:0710.4874 [hep-ph]].

- [71] R. S. Pasechnik, A. Szczurek and O. V. Teryaev, arXiv:0901.4187 [hep-ph].
- [72] K. Hagiwara, Q. Li and K. Mawatari, JHEP **0907**, 101 (2009) [arXiv:0905.4314 [hep-ph]].
- [73] L. D. Landau, Dokl. Akad. Nauk., USSR **60**, 207 (1948); C. N. Yang, Phys. Rev. **77**, 242 (1950).
- [74] M. Perelstein and A. Spray, arXiv:0907.3496 [hep-ph].
- [75] A. Djouadi, Phys. Rept. **459**, 1 (2008) [arXiv:hep-ph/0503173].
- [76] K. Cheung and W. Y. Keung, Phys. Rev. D **71**, 015015 (2005) [arXiv:hep-ph/0408335].